Phosphoglycerate mutase 1 regulates dNTP pool and promotes homologous recombination repair in cancer cells

Jia Qu,[1,2] Wenyi Sun,[2] Jie Zhong,[3] Hao Lv,[2] Mingrui Zhu,[2] Jun Xu,[2] Nan Jin,[2] Zuoquan Xie,[2] Minjia Tan,[2] Shu-Hai Lin,[3] Meiyu Geng,[2] Jian Ding,[1,2] and Min Huang[2]

[1]State Key Laboratory of Pharmaceutical Biotechnology, School of Life Sciences, Nanjing University, Nanjing 210023, China
[2]State Key Laboratory of Drug Research, Shanghai Institute of Materia Medica, Chinese Academy of Sciences, Shanghai 201203, China
[3]Department of Biochemistry and Molecular Cell Biology, Shanghai Key Laboratory for Tumor Microenvironment and Inflammation, Shanghai Jiao Tong University School of Medicine, Shanghai 200025, China

Glycolytic enzymes are known to play pivotal roles in cancer cell survival, yet their molecular mechanisms remain poorly understood. Phosphoglycerate mutase 1 (PGAM1) is an important glycolytic enzyme that coordinates glycolysis, pentose phosphate pathway, and serine biosynthesis in cancer cells. Herein, we report that PGAM1 is required for homologous recombination (HR) repair of DNA double-strand breaks (DSBs) caused by DNA-damaging agents. Mechanistically, PGAM1 facilitates DSB end resection by regulating the stability of CTBP-interacting protein (CtIP). Knockdown of PGAM1 in cancer cells accelerates CtIP degradation through deprivation of the intracellular deoxyribonucleotide triphosphate pool and associated activation of the p53/p73 pathway. Enzymatic inhibition of PGAM1 decreases CtIP protein levels, impairs HR repair, and hence sensitizes BRCA1/2-proficient breast cancer to poly(ADP-ribose) polymerase (PARP) inhibitors. Together, this study identifies a metabolically dependent function of PGAM1 in promoting HR repair and reveals a potential therapeutic opportunity for PGAM1 inhibitors in combination with PARP inhibitors.

Introduction

Tumor cells exhibit an altered energy metabolism different from most normal or differentiated cells, tending to metabolize glucose via aerobic glycolysis, also known as the Warburg effect (Hsu and Sabatini, 2008; Vander Heiden, 2011; Ward and Thompson, 2012). Such metabolic reprogramming provides cells with intermediates needed for biosynthetic pathways, including nucleotides, lipids, and nonessential amino acids, and thereby supports the anabolic requirements associated with unrestricted cell growth.

Accumulating studies have revealed that by controlling nutrient availability, altered metabolism may promote other cancer-essential functions, such as epigenetic regulation (Gut and Verdin, 2013), apoptosis avoidance (Bensaad et al., 2006), metastasis (Dupuy et al., 2015), and genomic stability (Jeong et al., 2013). Isocitrate dehydrogenase (IDH) mutations that occur in a broad spectrum of cancer types, such as glioma and acute myeloid leukemia, have recently been discovered to inhibit the TET family of enzymes via generation of an oncometabolite 2-hydroxyglutarate. As a result, IDH1 or IDH2 mutations in some tumor types have been linked with altered DNA methylation profiles that drive oncogenic growth (Figueroa et al., 2010; Turcan et al., 2012). Likewise, glucose-derived acetyl–coenzyme A is reported to influence histone acetylation via ATP-citrate lyase (Wellen et al., 2009). All these findings suggest that metabolic enzymes play much broader roles than currently understood.

Phosphoglycerate mutase 1 (PGAM1) is a glycolytic enzyme that catalyzes the conversion of 3-phosphoglycerate (3-PG) into 2-PG in glycolysis. PGAM1 expression is up-regulated in various human cancers, including breast cancer, lung cancer, prostate cancer, and glioblastoma (Durany et al., 2000; Chen et al., 2003; Sanzey et al., 2015), and enzymatic inhibition of PGAM1 impedes cancer growth. A recent study demonstrated that PGAM1 supports rapid cancer cell proliferation by coordinating glycolysis, serine generation, and the pentose phosphate pathway (PPP), which is associated with its metabolic function in controlling intracellular levels of 3-PG and 2-PG (Hitosugi

Correspondence to Min Huang: mhuang@simm.ac.cn; or Jian Ding: jding@simm.ac.cn

Abbreviations used: 6PGD, 6-phosphogluconate dehydrogenase; CDDP, cisplatin; ChIP, chromatin immunoprecipitation; CPT, camptothecin; CtIP, CTBP-interacting protein; DCA, dichloroacetate; dNTP, deoxyribonucleotide triphosphate; DSB, double-strand break; ECAR, extracellular acidification rate; HK, hexokinase; HR, homologous recombination; HU, hydroxyurea; IDH, isocitrate dehydrogenase; NHEJ, non-homologous end joining; PARP, poly(ADP-ribose) polymerase; PG, phosphoglycerate; PGAM1, phosphoglycerate mutase 1; PHGDH, phosphoglycerate dehydrogenase; PI, propidium iodide; PPP, pentose phosphate pathway; RPA, replication protein A; ssDNA, single-stranded DNA; WT, wild-type.

The Rockefeller University Press $30.00
J. Cell Biol. Vol. 216 No. 2 409–424
https://doi.org/10.1083/jcb.201607008

et al., 2012). Apart from this, the role of PGAM1 in cancer remains poorly understood.

To gain insights into biological processes involving PGAM1, we conducted a mass spectrometry–based proteomic study to globally characterize the signaling pathways affected by PGAM1 depletion. This effort identified multiple cellular processes that are potentially affected by PGAM1 inhibition; among them, we were particularly interested in the DNA damage response pathway (Fig. S1 A). This study aimed to investigate the potential role of PGAM1 in sustaining genomic integrity and elucidate its molecular mechanisms, which hopefully will unveil new implications for metabolism-based anticancer therapies.

Results

PGAM1 depletion selectively sensitizes cancer cells to DNA-damaging agents

To globally characterize the cellular processes that PGAM1 is potentially involved in, we conducted a proteomics study based on stable isotope labeling by amino acids in cell culture (SILAC), using scramble control and PGAM1 stably depleted HeLa cells to reveal differences in protein abundances. Indeed, PGAM1 knockdown led to abundance change in a set of proteins, including up-regulation of 233 proteins and down-regulation of 98 proteins (Student's *t* test, $P < 0.05$; 1.5-fold change in SILAC ratio). Further pathway analysis of the changed proteins revealed multiple pathways highly affected by PGAM1 silencing, including several metabolic pathways, as expected (Fig. S1 A). Among these affected pathways, we were particularly interested in the alterations of the intrinsic apoptotic signaling pathway in response to DNA damage and the regulation of cell cycle arrest, which together point to perturbations of the response to DNA damage.

To investigate the possible involvement of PGAM1 in sustaining genomic stability, we generated two more PGAM1 stably depleted cell lines using different shRNA sequences (shPGAM1#2 and #3) and exposed the cells to different DNA-damaging agents known to generate different forms of DNA lesions. Colony-formation assays showed that PGAM1-depleted HeLa cells (shPGAM1#1, #2, and #3) all exhibited hypersensitivity to camptothecin (CPT) or cisplatin (CDDP) but not to adriamycin (ADR) or etoposide (VP-16). The impact of individual PGAM1 shRNAs on cell sensitivity was associated with knockdown efficiency (Fig. 1, A and B; and Fig. S1 B), suggesting a PGAM1-associated defect.

The increased susceptibility to CPT and CDDP in PGAM1-depleted cells was recapitulated in non–small cell lung carcinoma NCI-H1299 and oral adenosquamous carcinoma CAL27 cell lines (Fig. S1, C and D). In line with the impeded cell growth measured by the colony-formation assay, we observed enhanced apoptotic cell death induced by CPT and CDDP in the three PGAM1 knockdown sublines (Figs. 1 C and S1 E), and the reconstitution of shRNA#1-resistant PGAM1 rescued the promoted apoptotic cell death in shPGAM1#1 cells at a level similar to that in scramble cells (Fig. 1 D). These results indicate that knockdown of PGAM1 selectively sensitizes cancer cells to DNA-damaging agents.

PGAM1 is required for the homologous recombination repair of DSBs

Although CPT and CDDP cause different forms of DNA lesions (i.e., topoisomerase I-DNA complex trapped by CPT and DNA intrastrand cross-link caused by CDDP), both agents are known to selectively kill proliferating cancer cells by causing replication-dependent DNA double-strand breaks (DSBs; Shao et al., 1999). Increased susceptibility to these two agents may indicate defects in DNA damage response specifically responding to DSBs. As such, we compared the occurrence of drug-induced DSBs in PGAM1-depleted cells and scramble control cells, using γH2AX as a surrogate marker. Cells were treated with 1 μM CPT for 2 h, refreshed with drug-free medium, and incubated for 2, 4, 6, or 8 h, which allowed us to monitor the kinetics of DSB change after treatment. γH2AX levels appeared similar in both cell lines after initial exposure to CPT for 2 h, suggesting comparable DNA lesions induced by the treatment (Fig. 2 A). Interestingly, we observed different kinetics of γH2AX levels after drug withdrawal. Whereas the scramble control cells showed a time-dependent γH2AX level decline after drug removal, γH2AX levels in PGAM1 knockdown cells were sustained until at least 8 h after CPT withdrawal (Fig. 2 A). This observation was recapitulated using an immunofluorescence assay to stain nuclear γH2AX foci (Fig. 2 B). These results suggested that knockdown of PGAM1 might impair cellular capacity in the repair of DSB lesions. For further confirmation, we used a comet assay to detect DNA damage in individual cells. A neutral lysis condition in this assay allowed us to detect DNA lesions mostly in the form of DSBs. A higher ratio of PGAM1 knockdown cells contained residual DSB lesions 8 h after drug withdrawal compared with scramble control cells, although DSBs were similarly induced upon initial treatment. Quantification of the remaining DNA lesions by measuring the tail moment in individual cells (50 cells per sample) showed similar results (Fig. 2 C). These results indicated a defect in DSB repair caused by the knockdown of PGAM1. In support of the deficient DSB repair, we observed that knockdown of PGAM1 increased the proportion of cells arrested at G2/M phase upon CPT treatment, suggesting delayed cell cycle progression caused by unrepaired DNA lesions (Fig. 2 D).

Replication-dependent DSB lesions are known to be predominantly repaired by homologous recombination (HR), a repair process requiring homologous DNA sequence as a template. To test whether PGAM1 knockdown cells were defective in HR repair, we chose a well-characterized reporter assay using a DR-U2OS human osteosarcoma cell line with a chromosomally integrated HR reporter gene containing an I-SceI recognition sequence. In this cell line, HR repair using a direct repeat within the reporter cassette as a template results in an intact GFP gene, which can be detected by flow cytometry (Pierce et al., 1999). This assay enabled us to discover that PGAM1 knockdown using two independent siRNAs remarkably decreased HR efficiency triggered by I-SceI, in which ATM inhibitor KU55933 was used as a positive control (Fig. 2 E). In contrast, PGAM1 silencing had no impact on non-homologous end joining (NHEJ) repair, as measured by a similar NHEJ reporter system using NHEJ-HeLa cells (Ogiwara et al., 2011). In this assay, DNA-PK inhibitor NU7441 significantly reduced the capacity of NHEJ repair, whereas PGAM1 knockdown barely affected it (Fig. 2 F). These data suggest the specific requirement of PGAM1 in HR repair, which echoes our findings in Fig. 1 that PGAM1 depletion did not affect cell sensitivity to VP-16 or ADR, as DNA lesions caused by these two agents were predominantly repaired by NHEJ repair (Wu et al., 2011). Together, these data identify a previously unappreciated role of PGAM1 in HR repair.

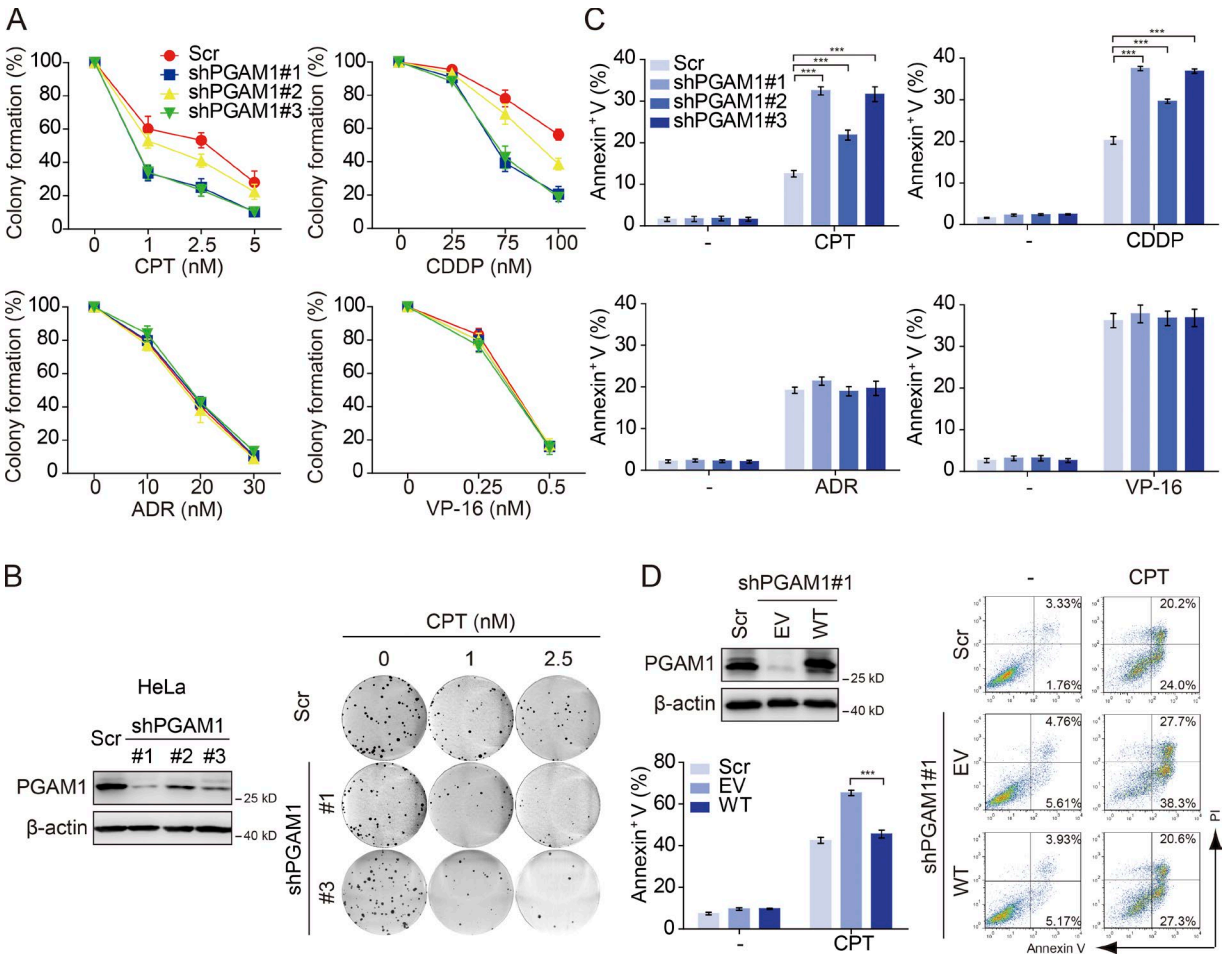

Figure 1. **PGAM1 depletion selectively sensitizes cancer cells to DNA-damaging agents.** (A and B) Clonogenic assay. PGAM1-depleted (shPGAM1#1, #2, #3) HeLa or scramble (Scr) cells were treated with indicated agents for 14 d. Knockdown efficiency was measured by immunoblotting. (C) Cell apoptosis assay. Cells as described in A were treated with CPT (1 µM), CDDP (10 µM), ADR (3 µM), or VP-16 (0.1 µM) for 48 h, and apoptotic cells were analyzed by Annexin V–PI dual staining. (D) Reconstitution of PGAM1 in PGAM1 knockdown cells. PGAM1 stable knockdown cells expressing shRNA-resistant WT PGAM1 or empty vector (EV) were treated with CPT (1 µM) for 48 h. Apoptotic cells were measured as in C. Error bars represent mean ± SD of triplicates. ***, $P < 0.001$.

Enzymatic activity of PGAM1 is required for HR repair

We next asked how PGAM1 was involved in HR repair. PGAM1 is mostly known as a glycolytic enzyme in glycolysis, although previous evidence also suggested the possibility of PGAM1 being present in the nucleus (Egea et al., 1992). However, we did not detect nuclear localization of PGAM1 in our experimental system (Fig. S2 A), which largely excluded its direct involvement in the repair machinery interacting with DNA lesions. We then asked whether the enzymatic activity of PGAM1 was required for its role in supporting HR repair. To this end, two well-characterized enzymatically inactive mutants of PGAM1, H186R and Y92F (Hitosugi et al., 2013; Zhang et al., 2016), were used to test the involvement of catalytic activity of PGAM1 in HR repair. As expected, the reconstitution of FLAG-tagged PGAM1 H186R or Y92F mutant failed to recover the decreased intracellular 2-PG levels caused by PGAM1 stable depletion (Fig. S2 B) as well as the glycolytic defect measured by extracellular acidification rate (ECAR; Fig. S2 C; Hitosugi et al., 2012). Interestingly, these two mutants also could not rescue the deficient repair responding to CPT treatment, as indicated by sustained γH2AX levels after drug withdrawal, similar to PGAM1 shRNA cells (Fig. 3 A). In contrast, reconstitution of wild-type (WT) PGAM1 resulted in the decline of γH2AX levels after drug removal, suggesting the recovery of repair efficiency. Similar results were obtained by detecting γH2AX foci formation (Fig. 3 B).

These results suggested that enzymatic activity of PGAM1 was required for HR repair. We hence introduced PGMI-004A, known as an enzymatic inhibitor of PGAM1, to confirm this result (Hitosugi et al., 2012). PGMI-004A treatment decreased intracellular 2-PG levels (Fig. S2 D) and HR repair efficiency (Fig. 3 C) without affecting NHEJ repair capacity (Fig. S2 F). Moreover, introduction of methyl-2-PG, a cell-permeable 2-PG derivative that is converted to 2-PG in cells (Hitosugi et al., 2012; Fig. S2 E), rescued the HR deficiency caused by PGAM1 siRNA (Fig. 3 C). These results together indicate that the enzymatic activity of PGAM1—namely, the activity in converting 3-PG to 2-PG—is required for HR repair.

In agreement with the deficient HR repair, reconstitution of the enzymatically inactive mutant PGAM1 failed to rescue increased cell apoptosis in PGAM1 knockdown cells, in contrast to the expression of WT PGAM1 (Fig. 3 D). Likewise, treatment with methyl-2-PG significantly recovered CPT-induced

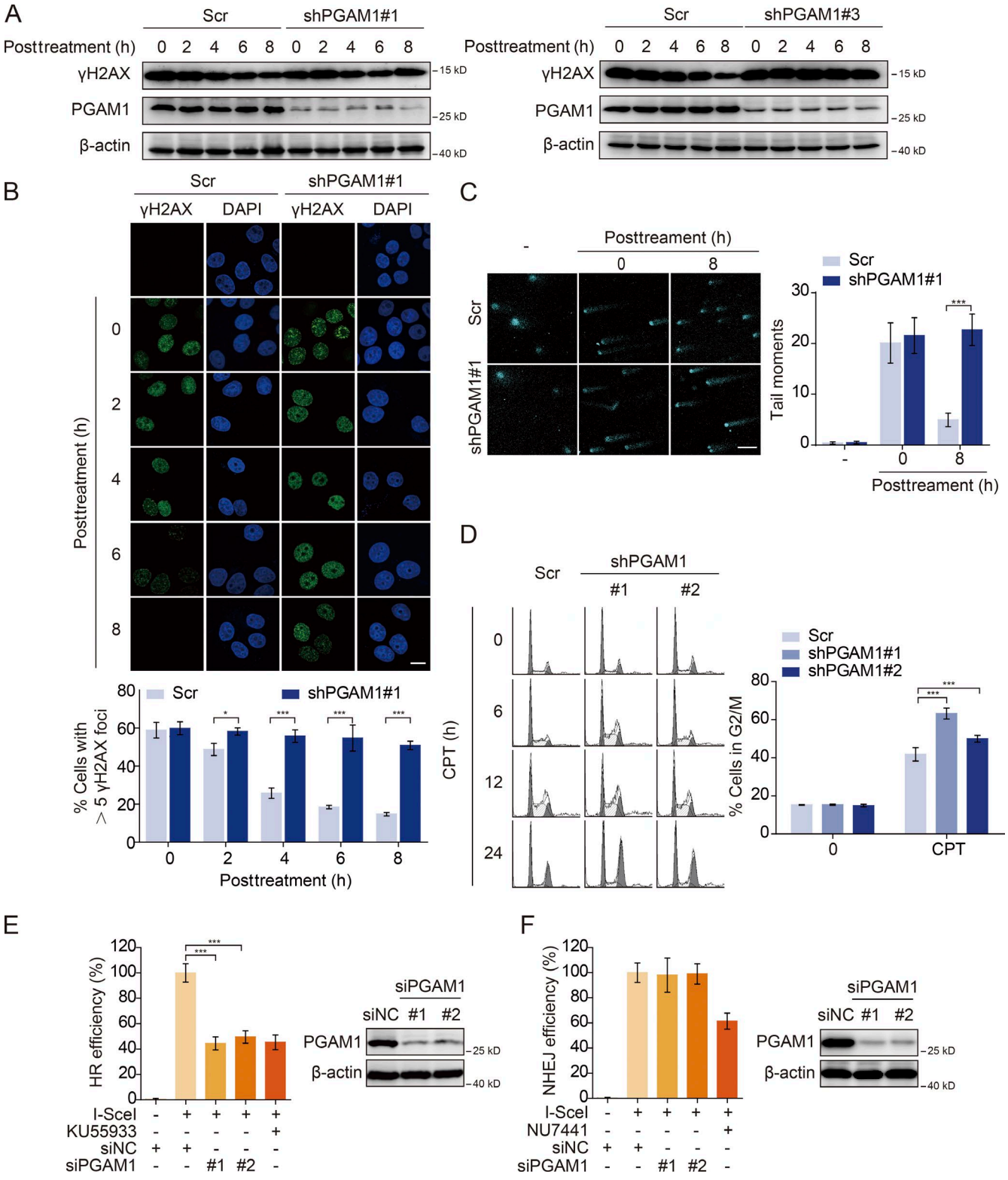

Figure 2. **PGAM1 is required for HR repair of DSBs.** (A and B) Kinetics of γH2AX levels and foci formation. HeLa shPGAM1#1, shPGAM1#3, or scramble (Scr) cells were treated with CPT (1 µM) for 2 h followed by drug-free culture for up to 8 h. γH2AX levels were detected by immunoblotting (A), and γH2AX foci were detected by immunofluorescence assay (B). Foci were quantified by counting at least 100 cells per sample. Bar, 10 µm. (C) Comet assay. Cells were treated as described in A before harvest for comet assay. Tail moments were quantified by measuring 50 cells per sample using CASP software. Bar, 100 µm. (D) Cell cycle analysis. HeLa shPGAM1#1, shPGAM1#2, or Scr cells were treated with CPT (10 nM) for 24 h, and the cell cycle profile was analyzed by flow cytometry. (E and F) HR and NHEJ repair assay. DR-U2OS (E) or NHEJ-HeLa (F) cells were transfected with indicated siRNAs for 24 h, followed by I-SceI transfection. KU55933 (10 µM) or NU7441 (10 µM) was added at the time of I-SceI transfection. GFP-positive cells were analyzed by flow cytometry 48 h later. Knockdown efficiency was measured by immunoblotting. siNC, negative control siRNA. Error bars represent mean ± SD of triplicates. *, $P < 0.05$; ***, $P < 0.001$.

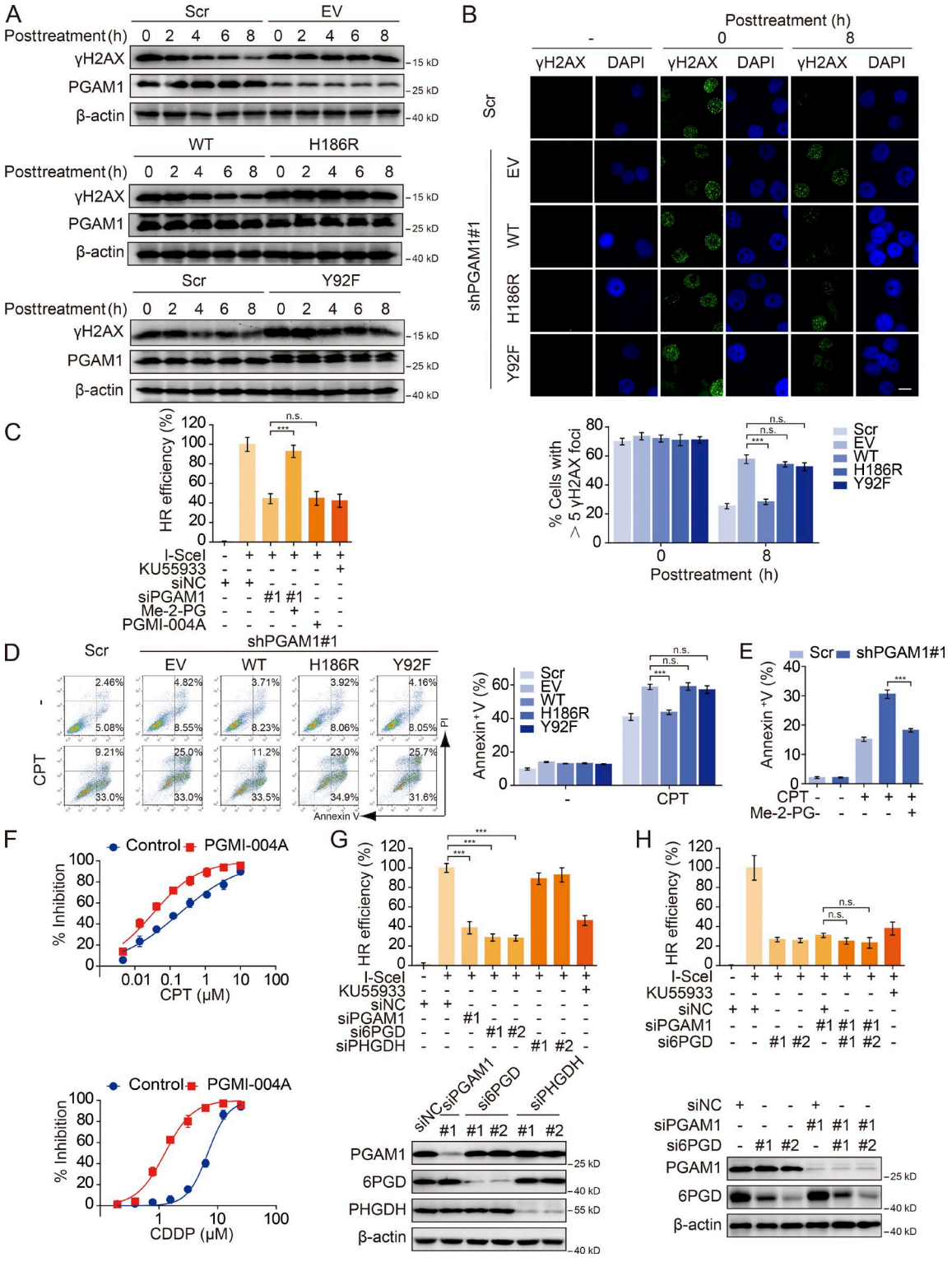

Figure 3. **PGAM1 enzymatic activity is required for HR repair.** (A and B) Kinetics of γH2AX levels and foci formation. PGAM1 stable knockdown cells (HeLa shPGAM1#1) reconstituted with empty vector (EV), WT, or mutant PGAM1 were treated with CPT (1 μM) for 2 h, followed by drug-free culture for up to 8 h, and subjected to immunoblotting (A) or immunofluorescence (B) assay. Foci were quantified by counting at least 100 cells per sample. Bar, 10 μm. (C) HR repair assay. DR-U2OS cells were pretreated with methyl-2-PG (Me-2-PG, 5 μM) or PGMI-004A (20 μM) for 24 h followed by I-SceI transfection. KU55933 (10 μM) was added at the time of I-SceI transfection. GFP-positive cells were analyzed by flow cytometry 48 h later. (D and E) Cell apoptosis assay. PGAM1-reconstituted cells as described in A or HeLa shPGAM1#1 cells were pretreated with Me-2-PG (5 μM) for 24 h. Apoptosis was then induced by CPT treatment for 48 h followed by Annexin V–PI dual staining. (F) Cell viability assay. HeLa cells were treated with CPT or CDDP alone or in combination with PGMI-004A (20 μM) for 72 h. Cell viability was measured by Sulforhodamine B assay. (G and H) HR repair assay. DR-U2OS cells were transfected with indicated siRNAs for 24 h followed by I-SceI transfection as in C. Knockdown efficiency was measured by immunoblotting. Error bars represent mean ± SD of triplicates. ***, P < 0.001; n.s., not significant.

apoptosis in PGAM1 knockdown cells (Fig. 3 E), and inhibition of PGAM1 activity using PGMI-004A sensitized HeLa cells to both CPT and CDDP (Fig. 3 F). These results further supported the requirement of catalytic activity of PGAM1 in repairing lethal DSB lesions during genomic stress.

PGAM1 has recently been reported to coordinate glycolysis, serine synthesis, and PPP flux by modulating the intracellular concentrations of 2-PG and 3-PG (Hitosugi et al., 2012). We next asked whether PGAM1 inactivation–associated HR defects resulted from functional deficiencies in glycolysis, serine metabolism, or PPP flux. Pharmacological inhibition of glycolytic flux using hexokinase 2 (HK2) inhibitor 2-DG, lactate dehydrogenase A (LDHA) inhibitor Oxamate, or pyruvate dehydrogenase kinase (PDHK) inhibitor dichloroacetate (DCA) did not sensitize HeLa cells to CPT or CDDP (Fig. S2 G), although glycolysis was clearly affected (Fig. S2 H). This result largely excluded the impact of impaired glycolysis on HR repair. We then introduced siRNAs to individually deplete 6-phosphogluconate dehydrogenase (6PGD) or phosphoglycerate dehydrogenase (PHGDH), whose activities are modulated by intracellular 2-PG or 3-PG levels (Hitosugi et al., 2012). Indeed, 6PGD rather than PHGDH depletion led to a reduction in HR efficiency (Fig. 3 G) without affecting NHEJ repair capacity (Fig. S2 I), similar to the phenotype of PGAM1 inactivation. Dual depletion of 6PGD and PGAM1 did not further impair HR repair compared with either PGAM1 or 6PGD depletion alone (Fig. 3 H), indicating that PGAM1 modulates HR repair by affecting 6PGD.

Enzymatic inhibition of PGAM1 impairs CtIP stability and DSB end resection

To understand how PGAM1 enzymatic activity and associated 6PGD activity are involved in HR repair, we looked into the procedure of HR repair, a multistep process starting with DSB end resection to expose single-stranded DNA (ssDNA) for the recruitment of ssDNA-binding protein complex Replication Protein A (RPA). We first examined ssDNA exposure after CPT treatment to indicate the capacity of DSB end resection. To this end, cells pulse-labeled with BrdU were exposed to CPT, and ssDNA generation was detected by anti-BrdU antibody under native conditions. CPT treatment for 2 h led to a remarkable increase in BrdU foci formation under native conditions, indicating the generation of massive ssDNA (Fig. 4 A). PGAM1 knockdown cells showed nearly half the reduction in CPT-induced ssDNA generation, although BrdU was equally incorporated, as indicated by BrdU staining under denatured conditions (Fig. 4 A). In line with the defect in ssDNA exposure, knockdown of PGAM1 resulted in impaired RPA foci formation, as probed by the immunostaining of RPA32 subunit (Fig. 4 B), and the defect in RPA foci formation was rescued by the expression of WT PGAM1 or methyl-2-PG treatment but not the expression of enzymatically inactive mutants (Fig. 4, C and D). Impaired RPA foci formation was associated with decreased RPA phosphorylation (Fig. S3 A), in agreement with the notion that ssDNA binding by the RPA complex is a prerequisite for its phosphorylation (Maréchal and Zou, 2015). Moreover, silencing of 6PGD instead of PHGDH resembled PGAM1 depletion in suppressing RPA foci formation (Fig. S3 B), and dual depletion of PGAM1 and 6PGD did not further strengthen the defect in RPA foci formation (Fig. S3 C). RPA-coated ssDNA is displaced by RAD51 to form nucleoprotein filaments that facilitate strand invasion and initiate the HR process (Symington, 2002). In additional to defective RPA recruitment to the damage site, we observed impaired RAD51 foci formation in PGAM1 knockdown cells (Fig. S3 D), further strengthening the deficiency in HR repair. Our results thus far suggested a hypothesis that PGAM1 is enzymatically involved in DSB end processing via its impact on the PPP pathway.

DSB end resection requires CtIP, which functions in 5′ strand resection in an MRN complex–dependent manner (Sartori et al., 2007). We hence examined the integrity of CtIP and MRN complex in PGAM1-inactivated cells. Knockdown of PGAM1 abolished CPT-induced CtIP foci formation (Fig. 4 E), whereas Mre11 foci indicating MRN complex recruitment appeared intact (Fig. S3 E). Further analysis of CtIP protein levels showed the decline of total CtIP levels in PGAM1-depleted cells, whereas levels of RAD51 and RPA32 were not affected (Fig. 4 F). Reconstitution of WT PGAM1 but not the enzymatically inactive mutants recovered CtIP levels (Fig. 4 G), suggesting a requirement of PGAM1 enzymatic activity in sustaining the protein level of CtIP. Consistently, inactivation of PGAM1 by PGMI-004A treatment decreased CtIP protein levels, which were restored by the addition of methyl-2-PG in PGAM1-depleted HeLa cells (Fig. S3 F). Consistent with our hypothesis, silence of 6PGD but not PHGDH resulted in a decrease in CtIP protein levels (Fig. 4 H).

The reduced CtIP seemed to result from proteasome degradation, as CtIP levels were recovered by MG132 treatment (Fig. S3 G) and PGAM1 depletion confers a similar destabilization of ectopically expressed FLAG-CtIP (Fig. S3 H). But mRNA levels of CtIP after PGAM1 or 6PGD knockdown were not affected (Fig. S3 I). We further examined the kinetics of CtIP protein level change on blockage of protein synthesis using cycloheximide (CHX), which allows measurement of the half-life of CtIP. CHX treatment led to decreases in CtIP protein levels in a time-dependent manner in scramble control cells, and PGAM1 depletion apparently promoted this process (Fig. 4 I). Collectively, these data imply that PGAM1 facilitated DSB processing by sustaining CtIP protein stability in an enzymatically dependent manner.

Decreased CtIP stability results from impaired dNTP synthesis

It remained unclear how PGAM1 and its modulated 6PGD activity were required for CtIP stability. 6PGD catalyzes the decarboxylating reduction of 6-phosphogluconate to generate ribose-5-phosphate as building blocks for nucleotide synthesis, yielding NADPH as a byproduct. In addition to a decreased $NADPH/NADP^+$ ratio (Fig. S4 A), knockdown of PGAM1 led to depletion of the deoxyribonucleotide triphosphate nucleoside (dNTP) pool, as indicated by a decrease in individual dNTP, namely dATP, deoxythymidine triphosphate (dTTP), and dCTP (Fig. 5 A). dGTP data were lacking because of technical difficulties in separating dGTP and ATP. Similar results were obtained by PGMI-004A treatment (Fig. 5 B). The imbalanced nucleotide metabolism was rescued by reconstitution of WT PGAM1 but not enzymatic inactive mutants (Fig. 5 A).

To test whether deficient nucleotide synthesis was responsible for CtIP destabilization, cells were treated with exogenous dNTP, which restored CtIP protein levels in PGAM1-depleted cells (Fig. 5 C). In agreement with this result, treatment with hydroxyurea (HU), which is known to decrease the production of dNTP by inhibiting ribonucleotide reductase (Thelander et al., 1985; Fig. S4 B), resulted in a reduction of CtIP levels that was reversed by MG132 treatment (Fig. S4 C). Along with the restored CtIP protein level, dNTP treatment also rescued impaired

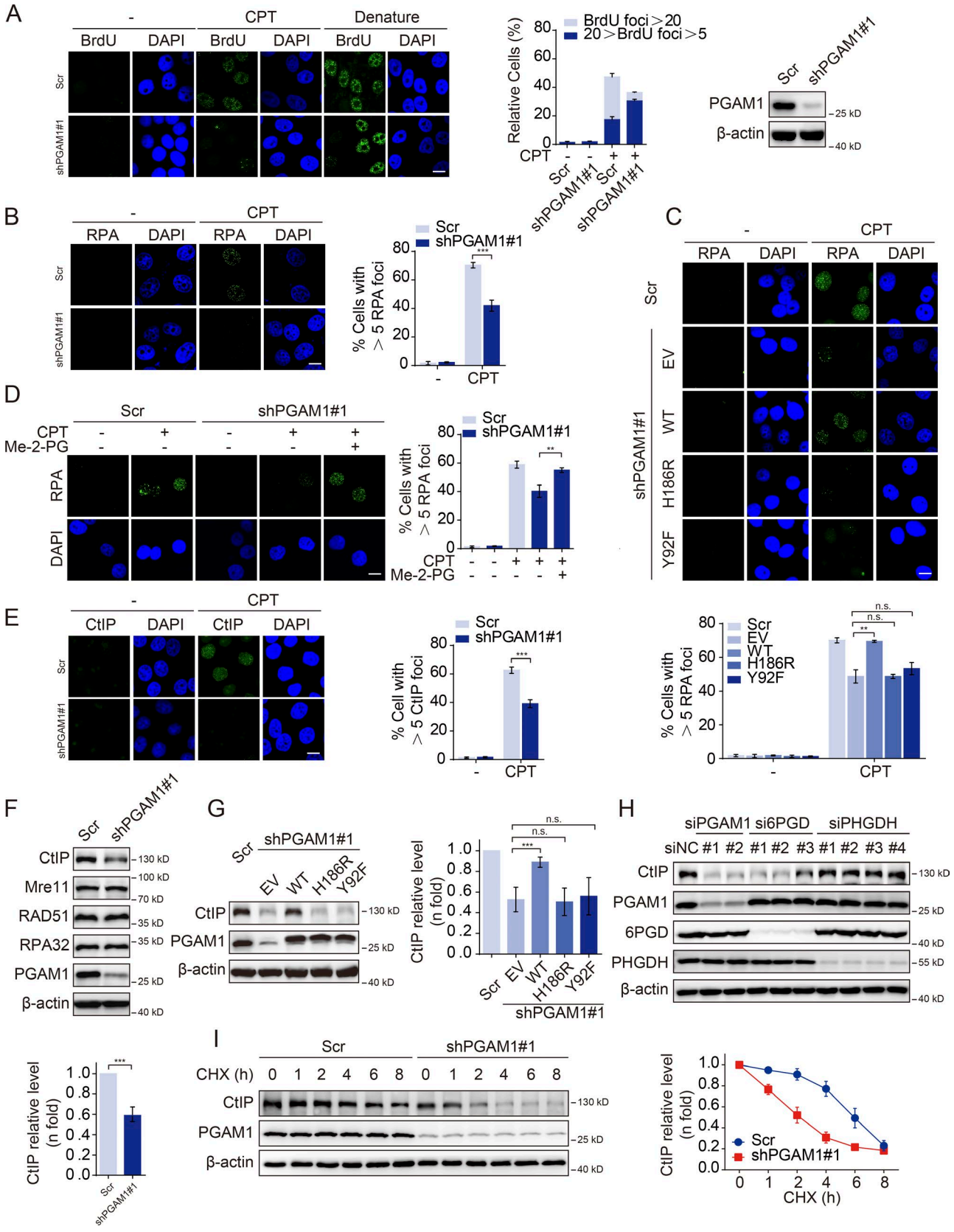

Figure 4. **Enzymatic inhibition of PGAM1 impairs CtIP stability and DSB end resection.** (A) ssDNA detection. HeLa shPGAM1#1 or scramble (Scr) cells were incubated with 20 μM BrdU for 36 h followed by CPT (1 μM) treatment for 2 h. ssDNA was detected using anti-BrdU antibody without denaturation. BrdU staining under denaturing conditions (2 M HCl) shows total BrdU incorporation. Knockdown efficiency was detected by immunoblotting. (B–D) RPA foci formation. Cells were exposed to CPT (1 μM) for 2 h, and RPA foci were detected by immunofluorescence assay. Foci were quantified by counting at least 100 cells per sample. HeLa shPGAM1#1 cells (B); HeLa shPGAM1#1 cells reconstituted with empty vector (EV), WT, or mutant PGAM1 (C); HeLa

RPA and CtIP foci (Fig. S4, D and E), thereby reactivating HR repair in PGAM1-depleted cells (Fig. 5 D). These results indicated that the defect in dNTP synthesis accounted for the destabilization of CtIP in PGAM1 knockdown cells.

A remaining puzzle was how dNTP pool deprivation affected CtIP stability. We noticed that suppression of nucleotide metabolism was reported to elevate p21 (Aird et al., 2013), which could prematurely activate ubiquitin ligase anaphase-promoting complex (or cyclosome APC/C-Cdh1; Wiebusch and Hagemeier, 2010). A recent study also reported that APC/C-Cdh1 controls CtIP stability in the DNA damage response (Lafranchi et al., 2014). We hence speculated that PGAM1 depletion might accelerate proteasome-mediated CtIP degradation by activating the p21-APC/C-Cdh1 pathway. To test this possibility, we first examined whether the APC/C-Cdh1 complex was involved in PGAM1-modulated CtIP degradation. In fact, decreased CtIP protein levels in PGAM1 stable knockdown cells was largely rescued by Cdh1 siRNA to levels similar to scramble cells (Fig. 5 E). In line with this result, we observed remarkably increased polyubiquitylation of CtIP in PGAM1-depleted cells compared with scramble cells (Fig. 5 F). These results supported our hypothesis that PGAM1 inhibition accelerated CtIP degradation by activating CtIP APC/C-Cdh1 E3 ubiquitin ligase.

We then examined whether p21 was involved in activating CtIP APC/C-Cdh1 E3 ubiquitin ligase. Immunoblotting and RT-qPCR analysis revealed that both mRNA and protein levels of p21 were elevated in PGAM1 knockdown cells (Fig. 5 G). 6PGD siRNA rather than PHGDH siRNA resembled the phenotype of PGAM1 silencing in increasing p21 levels (Fig. 5 G), consistent with their impact on CtIP protein levels. The p21 increase appeared to be dependent on dNTP pool deprivation, as the addition of exogenous dNTP partly reversed p21 protein levels in PGAM1-depleted cells (Fig. 5 H). Importantly, depletion of p21 in PGAM1 knockdown cells restored CtIP protein levels (Fig. 5 I) and HR repair proficiency (Fig. 5 J).

These results collectively suggest that knockdown of PGAM1 activates p21 transcription by perturbing the dNTP pool. Elevated p21 prematurely activates CtIP APC/C-Cdh1 E3 ubiquitin ligase, thereby accelerating proteasome-mediated CtIP degradation.

Impaired nucleotide metabolism activates p21 in a p53/p73-dependent manner

p21 appears to be an important molecular link between disturbed nucleotide metabolism and CtIP protein level control. We wished to understand how imbalanced dNTP levels caused p21 transcriptional up-regulation. The expression of p21 is tightly controlled by tumor suppressor protein p53 in response to a variety of stress stimuli (Zhao et al., 2000). Considering that the cell lines we used were deficient in p53 function (p53 destabilization in HeLa cells and homologous p53 deletion in NCI-H1299 cells), we tested the possible involvement of p73, a structural and functional homolog of p53 known to regulate p53 target genes, including p21, in a p53-deficient context (Irwin et al., 2003; Willis et al., 2003; Flores et al., 2005; Vayssade et al., 2005). Knockdown of p73 using three independent siRNAs abolished p21 levels in both HeLa (Fig. 6 A) and NCI-H1299 (Fig. 6 B) cells regardless of PGAM1 status, suggesting that p21 is tightly controlled by p73 in these cells. Importantly, although PGAM1 depletion barely affected total p73 protein levels, it increased the nuclear fraction of p73, suggesting the promoted nuclear translocation of p73 in PGAM1 stably depleted cells (Fig. 6 C). In agreement with this finding, chromatin immunoprecipitation (ChIP) assays using p73 antibody followed by qPCR analysis showed increased p73 recruitment in the promoter region of the p21 gene in PGAM1-depleted HeLa (Fig. 6 D) and NCI-H1299 (Fig. 6 E) cells, as probed by two independent pairs of primers specifically targeting the p21 gene promoter. Moreover, enhanced p73 enrichment in the p21 gene promoter in PGAM1 knockdown cells was reversed by dNTP supplementation (Fig. 6 D), suggesting that decreased dNTP levels were the cause of p73 activation. The nuclear translocation of p73 stimulated by decreased dNTP levels suggests p73 as a sensor of an imbalanced dNTP pool and plays an important role in coping with stress by transcriptionally activating p21.

Curious about the situation in p53 WT cancer cells, we expanded our study to p53 WT A549 and CAL51 cell lines. In both cell lines, the aforementioned findings caused by PGAM1 or 6PGD knockdown were largely recapitulated, including the elevation of p21 and the decrease of CtIP protein levels (Fig. 6 F). Interestingly, knockdown of p53 rather than p73 eliminated p21 levels in PGAM1-depleted cells, suggesting that p53 is required for p21 up-regulation upon PGAM1 inhibition (Fig. 6, G and H). In line with this result, subcellular fractionation of PGAM1 knockdown cells showed a marked increase in the nuclear fraction of p53, indicating promoted p53 translocation from cytoplasm to nuclei (Fig. 6 I). Further ChIP-qPCR analysis detected the increased recruitment of p53 in the p21 gene promoter region (Fig. 6 J). These results together suggested a model in which p53 and p73 play a key role in coping with the imbalance of dNTP levels in cancer cells by up-regulating p21, and in which p73 functions as a p53 counterpart in p53-inactive cells.

PGAM1 inhibition sensitizes BRCA-proficient breast cancer toward PARP inhibitors

Our results revealed a previously unappreciated role of PGAM1 in regulating HR repair that required its enzymatic activity. HR-deficient cancer, particularly BRCA1/2-deficient breast cancer, is exquisitely sensitive to the newly approved PARP inhibitor Olaparib (Tutt et al., 2010). Our findings may suggest a broader benefit of Olaparib expanded by PGAM1 enzymatic inhibition, as PGAM1 inhibitors have demonstrated therapeutic efficacy in cancer models and await further development (Hitosugi et al., 2012). To address this question, we used triple-negative breast cancer MDA-MB-231 cells bearing proficient BRCA1/2. A clonogenic assay showed that PGAM1-depleted MDA-MB-231 cells displayed considerably increased sensitivity to Olaparib compared with control cells (Figs. 7 A and S5 A). PGAM1 depletion remarkably increased apoptotic cell death caused by Olaparib treatment (Fig. 7 B), and reconstitution of WT PGAM1 but not the enzymatically inactive mutants

shPGAM1#1 pretreated with Me-2-PG (5 µM, 24 h; D). (E) CtIP foci formation. HeLa shPGAM1#1 cells were treated with 1 µM CPT for 2 h. CtIP foci were detected by immunofluorescence assay and quantified by counting at least 100 cells per sample. (F–I) CtIP protein level change. CtIP protein level was analyzed by immunoblotting. CtIP level was semiquantified by densitometry and normalized to untreated cells. HeLa shPGAM1#1 cells (F); HeLa shPGAM1#1 cells reconstituted with EV, WT, or mutant PGAM1 (G); HeLa cells transfected with indicated siRNAs for 48 h (H); HeLa shPGAM1#1 cells treated with CHX at 20 µM for indicated times (I). siNC, negative control siRNA. Bar, 10 µm. Error bars represent mean ± SD of triplicates. **, $P < 0.01$; ***, $P < 0.001$; n.s., not significant.

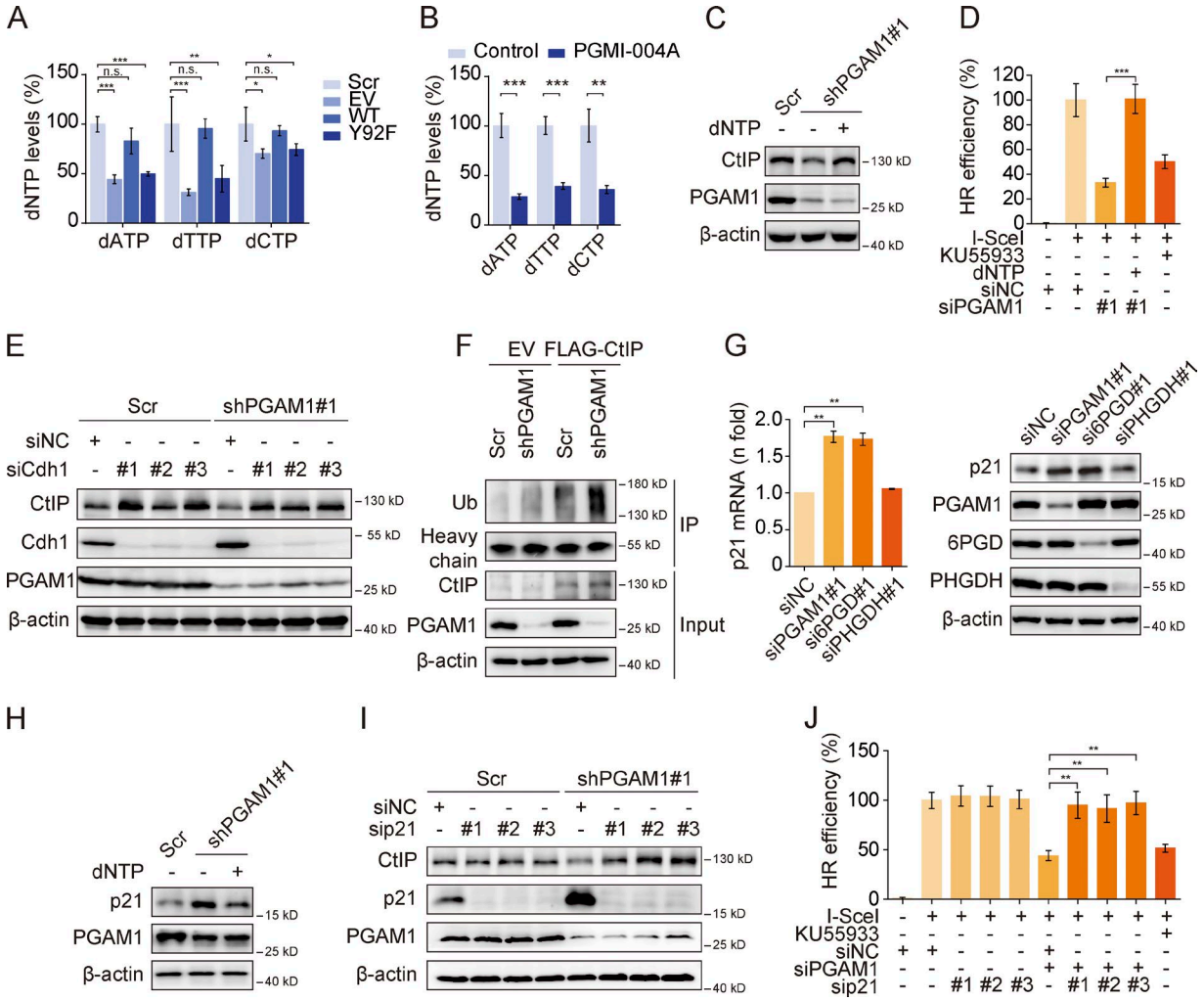

Figure 5. **Decreased CtIP stability results from deficient dNTP synthesis.** (A and B) dNTP level change. Intracellular individual dNTP levels were measured using LC-MS/MS analysis. (A) HeLa shPGAM1#1 cells reconstituted with empty vector (EV), WT, or mutant PGAM1; Scr, scramble cells. (B) HeLa cells treated with PGMI-004A (20 μM) for 24 h. (C) CtIP protein level change. HeLa shPGAM1#1 cells were treated with 100 μM dNTPs for 24 h before being subjected to immunoblotting. (D) HR repair assay. DR-U2OS cells were transfected with indicated siRNAs for 24 h followed by I-SceI transfection. dNTP (100 μM) or KU55933 (10 μM) was added at the time of I-SceI transfection. GFP-positive cells were analyzed by FACS analysis 48 h later. (E) CtIP protein level change. Cells transfected with indicated siRNAs for 72 h were harvested for immunoblotting analysis. (F) CtIP ubiquitylation assay. HeLa shPGAM1#1 or scramble (Scr) cells were transfected with FLAG-CtIP for 48 h, and MG132 (10 μM) was added 6 h before harvest. Cell lysates were subjected to immunoprecipitation using FLAG M2 beads followed by blotting with anti-ubiquitin antibody. (G and H) p21 level change. p21 mRNA or protein levels were examined using real-time PCR or immunoblotting analysis. (G) HeLa cells transfected with indicated siRNAs for 48 h. (H) HeLa shPGAM1#1 cells treated with dNTP (100 μM) for 24 h. (I) CtIP protein level change. Cells were transfected with indicated siRNAs for 48 h before being subjected to immunoblotting analysis. (J) HR repair assay. DR-U2OS cells were transfected with indicated siRNAs for 24 h. HR repair was assessed as in D. siNC, negative control siRNA. Error bars represent mean ± SD of triplicates. *, P < 0.05; **, P < 0.01; ***, P < 0.001; n.s., not significant.

H186R and Y92F rescued apoptosis induced by Olaparib (Figs. 7 C and S5 B). Consistently, combination with PGMI-004A sensitized MDA-MB-231 cells to Olaparib (Fig. 7 D).

We also proved this therapeutic potential using xenograft mice models. MDA-MB-231 scramble or shPGAM1#1 cells were subcutaneously injected into nude mice, and Olaparib (50 mg/kg) or vehicle was dosed daily for 2 weeks after tumor volume reached ~100–200 mm^3. MDA-MB-231 shPGAM1#1 tumors upon vehicle treatment showed impeded growth as well as decreased intratumoral 2-PG levels compared with control tumors (Figs. 7 E and S5 C), which supported the requirement of PGAM1 in conferring a growth advantage on cancer cells (Hitosugi et al., 2012). Notably, although tumor growth in the scramble group was not affected at all by Olaparib treatment, PGAM1 depletion substantially sensitized the tumor to Olaparib treatment (Figs. 7 E and S5 C). The increased response to Olaparib was associated with intratumoral levels of DSB lesions, as indicated by γH2AX levels 2 h after final dosing, as well as increased cleaved caspase 3 levels in the PGAM1-depleted group (Fig. 7, F and G). In support of the mechanism discovered in this study, the PGAM1-depleted group showed decreased CtIP protein levels (Fig. 7, F and G).

Our results suggest that PGAM1 inhibitor might be useful in combination with Olaparib in BRCA-proficient breast cancer. We hence measured the response of the MDA-MB-231 model to combined Olaparib and PGMI-004A treatment. Although Olaparib alone failed to show any therapeutic effect, its combination with PGMI-004A largely reduced intratumoral 2-PG levels (Fig. S5 D) and suppressed tumor growth (Fig. 7, H and I; and Fig. S5 D), suggesting Olaparib and PGMI-004A as a combination regimen for BRCA-proficient breast cancer.

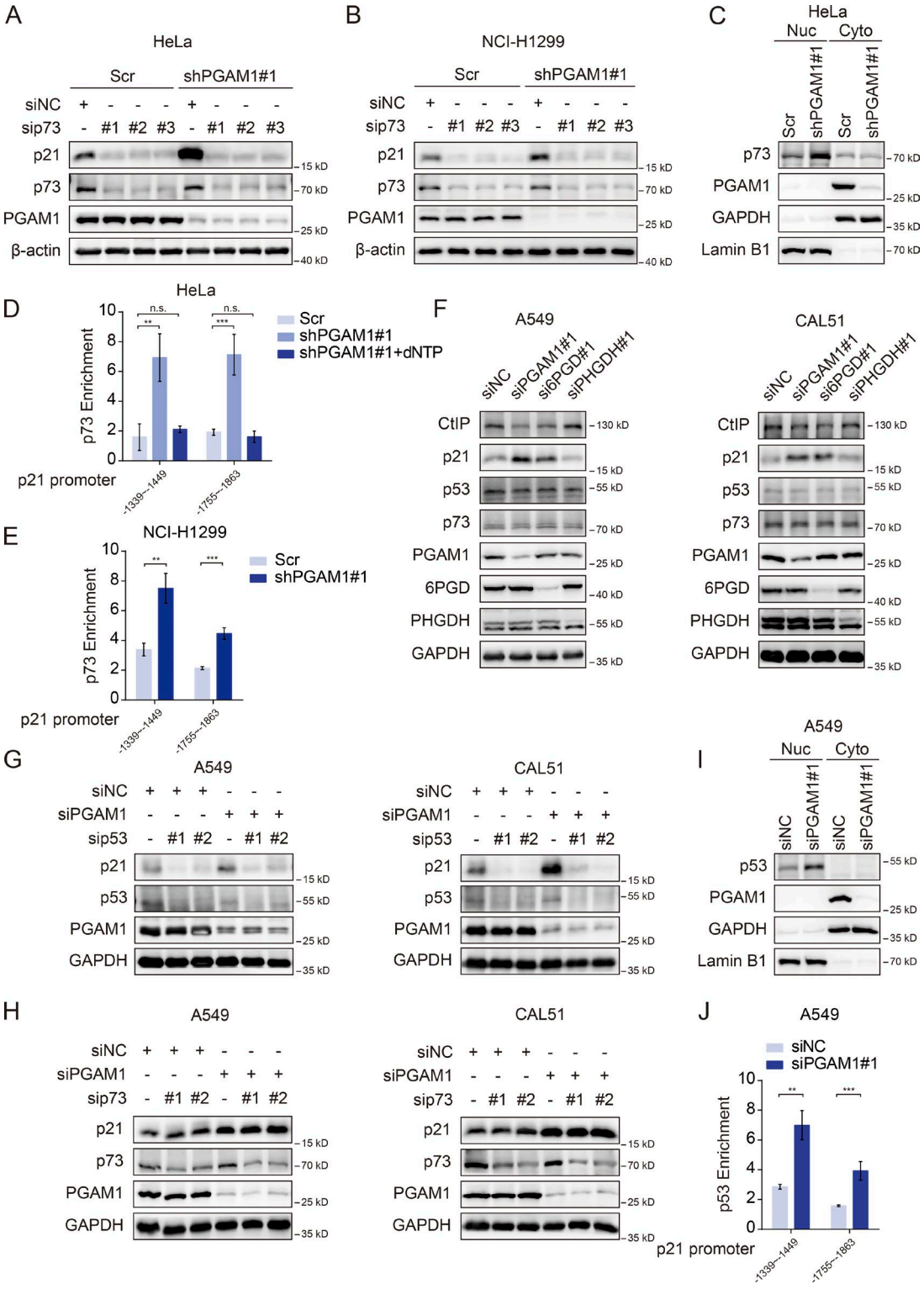

Figure 6. **Impaired nucleotide metabolism activates p21 in a p53/p73-dependent manner.** (A and B) p21 level change. HeLa shPGAM1#1 or NCI-H1299 shPGAM1#1 cells transfected with indicated siRNAs for 48 h were harvested for immunoblotting analysis. Scr, scramble cells. (C) Subcellular localization of p73 in PGAM1 knockdown HeLa cells. Nuc, nuclear fraction; Cyto, cytoplasmic fraction. (D and E) p73 enrichment in p21 promoter detected by ChIP assay. HeLa shPGAM1#1 or NCI-H1299 shPGAM1#1 cells were subjected to ChIP assay using anti-p73 antibody followed by qPCR analysis using primers targeting indicated p21 promoter region. dNTP at 100 µM was added 24 h before harvest. (F–H) p21 level change. A549 or CAL51 cells transfected with indicated siRNAs for 48 h were harvested for immunoblotting analysis. (I) Subcellular localization of p53 in PGAM1 knockdown A549 cells. (J) p53 enrichment in p21 promoter detected by ChIP assay. A549 cells transfected with indicated siRNAs for 48 h were subjected to ChIP assay using anti-p53 antibody followed by qPCR analysis as described in D. siNC, negative control siRNA. Error bars represent mean ± SD of triplicates. **, $P < 0.01$; ***, $P < 0.001$; n.s., not significant.

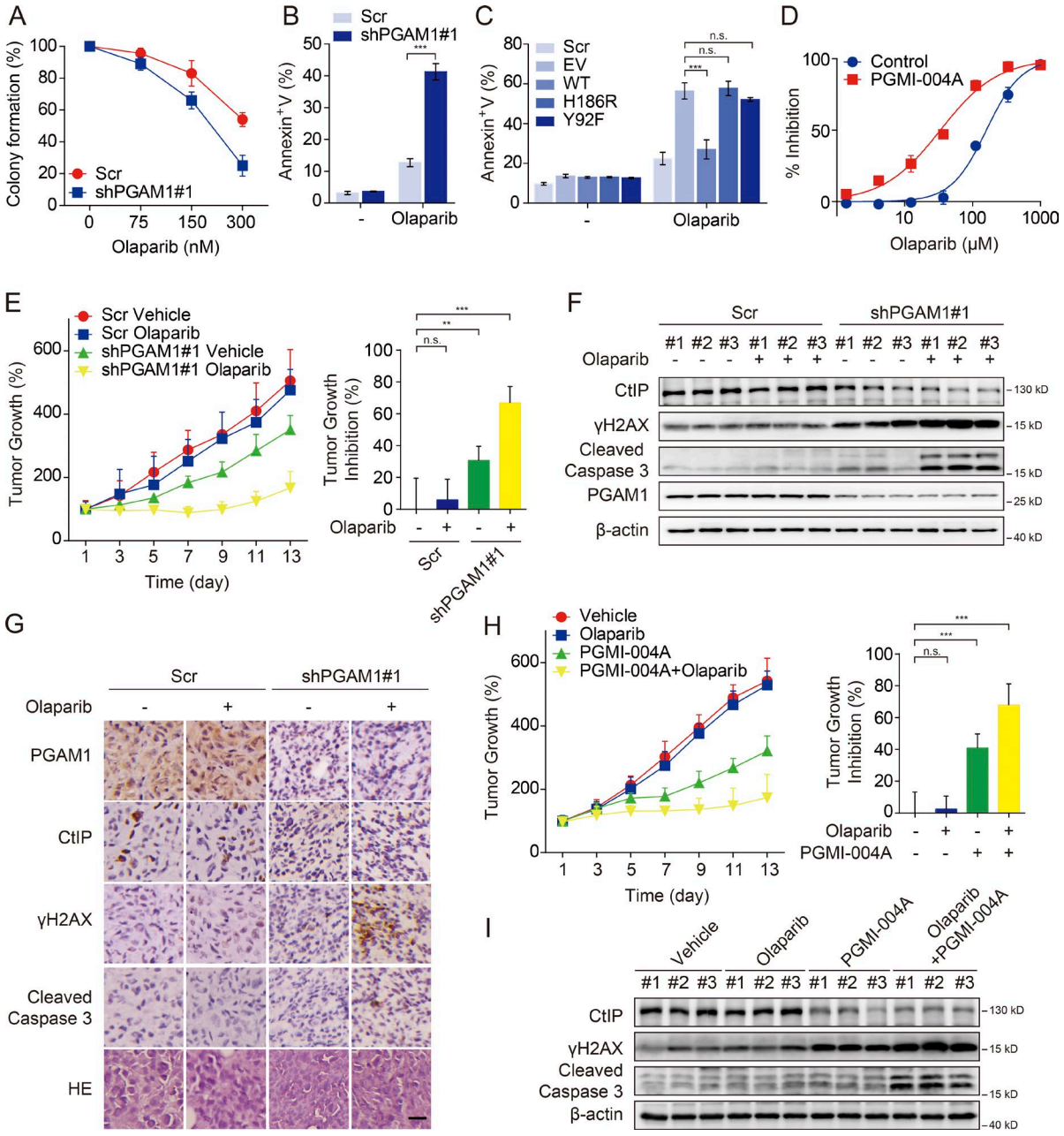

Figure 7. **PGAM1 inhibition sensitizes BRCA-proficient breast cancer toward PARP inhibitors.** (A) Clonogenic assay. MDA-MB-231 shPGAM1#1 or scramble (Scr) cells were treated with Olaparib at indicated concentrations for 14 d. (B and C) Cell apoptosis assay. Cells were exposed to Olaparib (30 μM) for 48 h, and apoptotic cells were detected by Annexin V–PI dual staining. (B) MDA-MB-231 shPGAM1#1 cells. (C) MDA-MB-231 shPGAM1#1 cells transfected with empty vector (EV), WT, or mutant PGAM1 for 24 h. (D) Cell viability assay. MDA-MB-231 cells were treated with Olaparib alone or in combination with PGMI-004A (20 μM) for 72 h. Cell viability was measured by Sulforhodamine B assay. (E–I) Tumor growth inhibition in vivo. Mice bearing indicated tumors were dosed with Olaparib (50 mg/kg) alone or in combination with PGMI-004A (50 mg/kg) daily for 14 d ($n = 6$). Tumor volume was measured every other day, and tumor growth inhibition at endpoint was measured (E and H). Tumor tissues collected at 2 h after the last dosing were subjected to immunoblotting (F and I) or immunohistochemistry (G) analysis. Bar, 20 μm. **, $P < 0.01$; ***, $P < 0.001$; n.s., not significant.

Discussion

Glycolytic enzymes are known to catalyze aerobic glycolysis to sustain the bioenergetic and biosynthetic demands of cell proliferation (Hsu and Sabatini, 2008; Vander Heiden, 2011; Ward and Thompson, 2012). Apart from this, our understanding of their roles in cancer remains very limited. This study revealed a metabolism-associated function of PGAM1 in HR repair, which stems from its role in maintaining intracellular dNTP pool. The balance of dNTP pool is known to affect a variety of cellular processes, including those essential for sustaining genomic stability. dNTP pool imbalance may lead to higher mutation rates, escaped S-phase checkpoints, and impaired DNA repair (Kumar et al., 2010), causing genomic instability and sensitizing cancer cells to chemotherapies (Lin et al., 2004). However, the detailed molecular basis remains unclear. One study has reported that perturbation of dNTP pool influences mispair extension by mutator DNA polymerases (Williams et al., 2015). Our results advanced the current understanding by showing that dNTP balance is essential for DSB end resection in HR repair by affecting CtIP stability (Fig. 8).

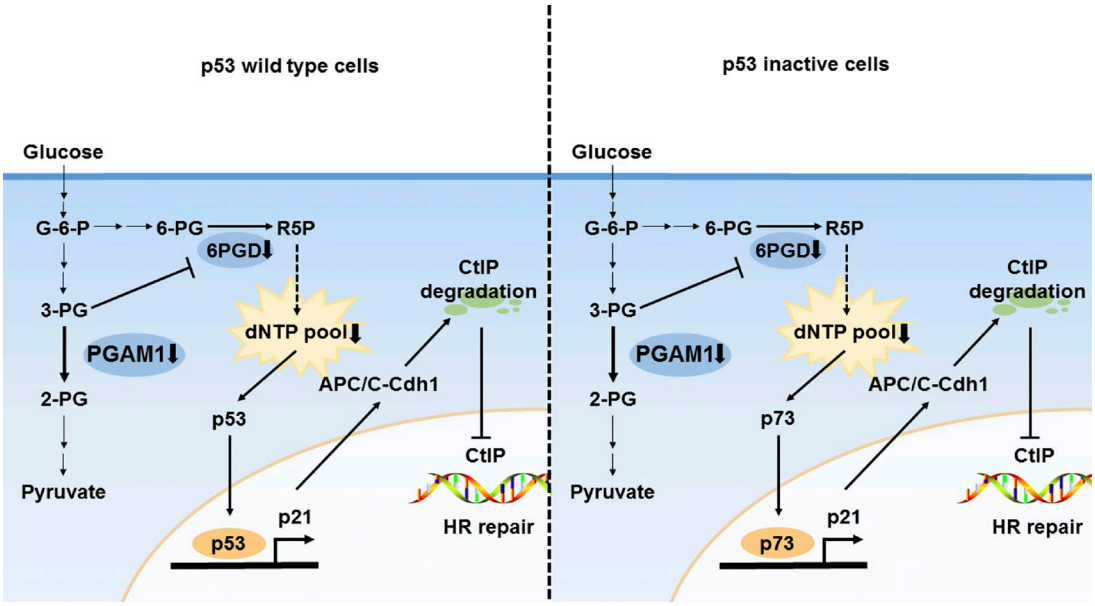

Figure 8. **Schematic model showing that PGAM1 promotes HR repair in a metabolic-dependent manner.** Imbalance of dNTP caused by PGAM1 inhibition promotes the translocation of p53 into nuclei and in turn activates p21 in p53 WT cancer cells, where p73 functions as a p53 counterpart in p53 inactive cells. Up-regulated p21 leads to CtIP degradation by activating the APC/C-Cdh1 complex and thereby impairing HR repair.

This study also provides evidence for a better understanding of how dNTP pool imbalance may affect CtIP protein levels. We identify p53/p73-dependent transcriptional activation of p21 as the important molecular link between dNTP pool deprivation and declined CtIP stability (Fig. 8). In line with a previous study showing that APC/C-Cdh1 ubiquitin ligase activity is prematurely activated as part of a p53/p21-dependent long-term response to DNA damage (Wiebusch and Hagemeier, 2010) and APC/C-Cdh1 regulates degradation of CtIP, we have shown that both p21 and APC/C-Cdh1 are required for accelerated CtIP degradation upon dNTP pool deprivation. Another study suggested that a decrease in dNTP levels causes cells to undergo senescence, which is associated with up-regulation of p21 (Aird et al., 2013). We advance this insight by showing that p21 is transcriptionally activated by p53 or p73 in coping with dNTP pool imbalance, and that p73 functions as a p53 counterpart in p53-inactivated cells. Interestingly, the activation of p53/p73 is indicated by promoted nuclear entry and chromatin recruitment to p21 promoter region. Together, these data suggest a model in which p53/p73 function as sensors of the cytoplasmic dNTP pool to cope with nucleotide metabolism disorders.

Obviously, a defect in nucleotide synthesis was not the only link connecting metabolic molecules to the DNA damage response. Fumarase, a mitochondrial metabolic enzyme involved in the tricarboxylic acid cycle, is localized to the nucleus in response to DNA damage and exhibits a metabolically dependent role in maintaining genomic integrity (Yogev et al., 2010). In contrast, ATM, a key player in DNA damage response, activates the PPP pathway by stimulating G6PD to promote an antioxidant response (Cosentino et al., 2011). TP53-induced glycolysis and apoptosis regulator (TIGAR) regulates DNA damage and repair through inhibition of glycolysis and enhancement of the PPP pathway (Yu et al., 2015). Moreover, GAPDH and pyruvate kinase M2 were reported to be ATM/ATR substrates (Matsuoka et al., 2007). All this evidence highlights metabolic control as an important event in the DNA damage response. In the case of CtIP-associated mechanistic insights, there remain discrepancies that need further characterization. CtIP is known to control the initiation of DNA end resection in HR promotion in both S and G2 phases and microhomology-mediated end joining in G1 phase in chicken cells. Meanwhile, Aparicio et al. (2016) have shown that the MRN complex, CtIP, and BRCA1 are required for efficient removal of VP-16–induced Top2-DNA adducts using cell-free extracts from *Xenopus laevis* eggs (Nakamura et al., 2010). This appears consistent with the study showing that CtIP depletion sensitized G1 phase cells to VP-16 (Quennet et al., 2011). However, we did not observe an impact of CtIP depletion on VP-16 sensitivity in the cells we tested. These disparities were probably caused by the heterogeneous genetic background of the cancer cells and need further characterization.

The close interplay between the DNA damage response and cell metabolism suggests new therapeutic strategies composed of DNA-damaging agents and metabolic inhibitors. Glycolysis inhibitors, such as HK2 inhibitor 2-DG, are reported to enhance the clinical efficacy of chemo- or radiotherapy (Zhao et al., 2013). We herein reveal a possibility of using PGAM1 inhibitor to sensitize PARP inhibitors, thereby expanding the benefits of PARP inhibitor to BRCA1/2-proficient breast cancer, in particular triple-negative breast cancer lacking effective therapies. In support of our mechanistic findings, CtIP expression has recently been suggested as a response biomarker for PARP inhibitors (Wang et al., 2016). In addition to PGAM1 inhibitors, our results also suggest the therapeutic potential of 6PGD and even inhibitors of PPP flux. Interestingly, similar to PGAM1 (Durany et al., 2000), 6PGD is up-regulated in many cancers (Jonas et al., 1992). 6PGD activity is reported as a reliable prognostic biomarker for primary breast cancer (Brocklehurst et al., 1986), suggesting the potential of 6PGD inhibition in the 6PGD-positive breast cancer subset in a combination of PARP inhibitors. This study may also provide an example to identify new opportunities for metabolic inhibitors, most of which still lack well-defined responsive subsets.

Materials and methods

Cell lines

HeLa, NCI-H1299, MDA-MB-231, CAL27, and A549 cells were obtained from ATCC, and CAL51 cells were obtained from Deutsche Sammlung von Mikroorganismen und Zellkulturen. DR-U2OS cells were gifted by M. Jasin and H. Masai (Memorial Sloan-Kettering Cancer Center, New York, NY) and NHEJ-HeLa cells were provided by D. Chowdhury (Dana-Farber Cancer Institute, Boston, MA). All cell lines were authenticated by the short tandem repeat analysis (Genesky Biotechnologies) and were maintained in appropriate culture medium as the suppliers suggested.

Antibodies

The following antibodies were used in this study: anti-PGAM1 (NBP1-49532; Novus Biologicals), anti-CtIP (sc-271339; Santa Cruz Biotechnology, Inc.), anti-Mre11 (ab214; Abcam), anti–H2AX-pS139 (9718; Cell Signaling Technology), anti–β-actin (60008-1-Ig; Proteintech), anti–Lamin B1 (12987-1-AP; Proteintech), anti-GAPDH (60004-1-Ig; Proteintech), anti-RPA32 (ab2175; Abcam), anti–RPA32-pS4S8 (NBP1-23017; Novus Biologicals), anti-BrdU (5292; Cell Signaling Technology), anti-Cdh1 (ab3242; Abcam), anti-p21 (2947; Cell Signaling Technology), anti-RAD51 (sc-8349; Santa Cruz Biotechnology, Inc.), anti-PGD (sc-398977; Santa Cruz Biotechnology, Inc.), anti-PHGDH (ab57030; Abcam), anti-IgG (2729; Cell Signaling Technology), anti-Histone H3 (4620; Cell Signaling Technology), anti-p53 (9282; Cell Signaling Technology), anti-p73 (ab202474; Abcam), and anti–Cleaved Caspase-3 (9661; Cell Signaling Technology).

Plasmid, shRNA, and siRNA transfection

PGAM1 stably depleted cells were generated using pLKO.1 lentiviral system (Addgene). The target sequences of shRNAs were as follows: Scramble (Scr), 5′-CAAATCACAGAATCGTCGTAT-3′; shPGAM1#1, 5′-CCATCCTTTCTACAGCAACAT-3′; shPGAM1#2, 5′-CCTGTGAGAGTCTGAAGGATA-3′; and shPGAM1#3, 5′-CGCCTCAATGAGCGGCACTAT-3′.

Coding sequences of FLAG-PGAM1 and indicated mutants were cloned to pCDNA3.1 vector. Nonsense point mutations to the underlined nucleotides 5′-CCA<u>C</u>CC<u>A</u>TT<u>T</u>TACAGCAACAT-3′ in the corresponding coding sequence of PGAM1 in the pCDNA3.1 plasmid confer resistance to shRNA#1 silencing. WT or mutant PGAM1 reconstituted cells were stable lines generated by Lipofectamine 2000 (Invitrogen) transfection followed by G418 selection. The lines used in this study were selected monoclones with expression levels comparable to those of endogenous PGAM1.

For siRNA transfection, cells were plated at 30–60% confluence in OPTI-MEM serum-free medium and transfected with a specific siRNA duplex using Lipofectamine RNAiMAX (Invitrogen) according to the manufacturer's instructions. siRNAs were ordered as reverse-phase HPLC–purified duplexes from Sigma-Aldrich and Shanghai GenePharma Co., Ltd. The sequences were as follows: negative control siRNA (siNC), 5′-UUCUCCGAACGUGUCACGUTT-3′; siPGAM1#1, 5′-CGACUGGUAUUCCCAUUGUTT-3′; siPGAM1#2, 5′-GUCCUGUCCAAGUGUAUCUTT-3′; si6PGD#1, 5′-GGCCAGAACUUAAUUCUGATT-3′; si6PGD#2, 5′-CUGGUGACAUCAUCAUUGATT-3′; si6PGD#3, 5′-GCUGCAUCAUUAGAAGUGUTT-3′; siPHGDH#1, 5′-CUUAGCAAAGAGGAGCUGAUA-3′; siPHGDH#2, 5′-CAGACUUCACUGGUGUCAGAU-3′; sip21#1, 5′-GAUGGAACUUCGACUUUGUTT-3′; sip21#2, 5′-CCUCUGGCAUUAGAAUUAUTT-3′; siCdh1#1, 5'-GGAUUAACGAGAAUGAGAATT-3'; siCdh1#2, 5'-AAUGAGAAGUCUCCCAGUCAGTT-3'; siCdh1#3, 5'-GCAACGAUGUGUCUCCCUATT-3'; sip73#1, 5′-CCAUGCCUGUUUACAAGAATT-3′; sip73#2, 5′-CCAUCCUGUACAACUUCAUTT-3′; sip73#3, 5′-GUGGAAGGCAAUAAUCUCUTT-3′; sip53#1, 5′-GUACCACCAUCCACUACAATT-3′; and sip53#2, 5′-GUAAUCUACUGGGACGGAATT-3′.

Proteome quantification

Proteins from heavy and light amino acid–labeled cells were extracted, mixed equally, and digested with trypsin. Peptide mixture offline fractionation was performed on with a BEH C18 column by 0% to 100% buffer B (98% acetonitrile, pH 10.0 adjusted with $NH_3{\cdot}H_2O$) in buffer A (2% acetonitrile, pH 10). The obtained peptide fractions were subjected to nanoflow HPLC-MS/MS analysis using an Orbitrap Fusion mass spectrometer coupled to an EASY-nLC1000 HPLC system (Thermo Fisher Scientific). Raw MS files were analyzed by MaxQuant against the UniProt Human database using default parameters. Gene ontology enrichment analysis was performed using ClueGo of the Cytoscape 3.4.0 bioinformatics tool. The mass spectrometry raw data were deposited and are publicly accessible on the iProX database under project number IPX00081700.

Cell viability assay

Cells were seeded in 96-well plates overnight and treated with the indicated drugs. Sulforhodamine B assay (Thermo Fisher Scientific) was performed after incubation for 72 h. The absorbance (optical density [OD]) was read at a wavelength of 560 nm on an ELISA plate reader. The growth inhibition rate was calculated according to (OD treated/OD control) × 100%, in which untreated cells served as the control. Data represent the mean from triplicates.

Apoptosis assay

Apoptotic cells were measured by Annexin V and propidium iodide (PI) dual staining using the Annexin V–FITC Apoptosis Detection kit (BD) followed by flow cytometry analysis. 10,000 cells per sample were collected for analysis and quantification. Cells with positive Annexin V staining (Annexin V^+) were considered apoptotic cells.

Immunoblotting analysis

Cells were lysed using preheated 2% SDS by vortexing vigorously for 2–3 s at maximum speed, followed by boiling for 30 min. The same amount of proteins were subjected to SDS-PAGE, transferred to PVDF membranes (Immobilon-P; EMD Millipore), and blocked for 1 h at RT with 3% milk in 1× Tris-buffered saline Tween-20 (TBST; 25 mM Tris, 150 mM NaCl, and 2 mM KCl, pH 7.4, supplemented with 0.2% Tween-20). Blotting was performed with primary antibodies at 4°C overnight. After washing the membranes with TBST three times for a total of 30 min, HRP-conjugated secondary antibodies were incubated at RT for 1 h. The membranes were washed for 30 min with TBST three times, and proteins were visualized with an enhanced chemiluminescence assay (Thermo Fisher Scientific) or Femto chemiluminescence assay (Thermo Fisher Scientific).

Cell cycle analysis

Cells were washed with PBS and fixed with 70% ethanol for later use. Cells were rehydrated with PBS, resuspended in 500 µl of PI/RNase staining solution (Immunostep), and incubated for 20 min at RT in the dark. 10,000 cells were collected per sample and were analyzed using a FACSCalibur flow cytometer.

Comet assay

DSBs were measured using neutral comet assay as previously reported (Fairbairn et al., 1995). 2×10^5 trypsinized cells were pelleted and suspended in 1 ml ice-cold PBS followed by the standard protocol. 50 µl of

cell suspension was mixed with 100 µl of 0.75% prewarmed low-melting point agarose and dropped slowly on a fully frosted slide precoated with 0.75% agarose. After solidifying, the slides were submerged in precold (4°C) lysis buffer (2.5 M NaCl, 100 mM EDTA, 1% Sarcosyl, 10 mM Tris, 1% Triton X-100, and 10% DMSO) at 4°C for 1 h followed by unwinding DNA in precold electrophoresis buffer (8.9 mM Tris, 8.9 mM orthoboric acid, and 0.2 mM EDTA, pH 7.5) at 4°C for 30 min. Electrophoresis was performed at 2 V/cm for 10 min. Cells were stained with DAPI, and images were captured using a laser scanning confocal microscope Fluoview FV1000 (Olympus) with a UPlansApo 20×/0.75 (Olympus) at RT. Images were processed using an FV1000 Viewer (Olympus). To quantify the level of DNA damage, 50 cells of each sample were analyzed for tail moment by CASP software.

HR and NHEJ repair assay

HR repair assays were performed as previously described using the DR-U2OS reporter cell line (Pierce et al., 1999). 10,000 cells were collected per sample for quantification. NHEJ assay was performed as described previously (Ogiwara et al., 2011) using the NHEJ-HeLa reporter cell line. KU55933 or NU7441 (10 µM; Sigma-Aldrich) was added at the time of I-SceI introduction as positive controls. GFP-positive cells were quantified by flow cytometry.

Immunofluorescence microscopy

For foci formation, cells were permeabilized with 0.5% Triton X-100 for 5 min before fixation, and then treated with primary and secondary antibodies. For ssDNA detection, BrdU incorporation was performed as described in Huang et al. (2010). ssDNA was detected using anti-BrdU antibody without denaturation. Total BrdU incorporation was determined under denatured conditions (2 M HCl). Images were captured using a laser scanning confocal microscope (Fluoview FV1000) with a UPlansApo 100×/1.40 oil (Olympus) at RT and processed using an FV1000 Viewer. At least 100 cells were counted per sample for quantification, and cells containing more than five foci were considered positive.

Subcellular fractionation

Cytoplasmic and nuclear protein extracts were prepared using a nuclear and cytoplasmic protein extraction kit (Bio-Equip) according to the manufacturer's instructions. In brief, the cells were washed with ice-cold PBS and lysed in cell lysis buffer containing 10 mM Hepes, pH 7.9, 10 mM KCl, 0.1 mM EDTA, 1 mM DTT, 0.4% IGEPAL, and 1 mM PMSF for 20 min on ice. After centrifugation, the supernatants (corresponding to the cytoplasmic extracts) were collected, and the nuclei pellets were washed with ice-cold cell lysis buffer and resuspended in nuclear extraction buffer (0.4 M NaCl, 20 mM Hepes, pH 7.9, 1 mM EDTA, 1 mM DTT, and 1 mM PMSF). After vigorous shaking for 30 min at 4°C, nuclear extracts were collected by centrifugation.

Intracellular 2-PG measurement

A 2-Phosphoglycerate Colorimetric/Fluorometric Assay kit (BioVision) was used to measure intracellular 2-PG concentrations. Cells were collected by a scraper, washed with PBS, and lysed with ice-cold 2-PG assay buffer. The extracts were spun down to remove cell debris, and the supernatant was reacted with working buffer according to the manufacturer's instructions. The fluorescence (excitation, 535 nm; emission, 587 nm) from the reaction mixture was measured with plate reader.

Ubiquitination assay

Cells were transfected with pCDNA3.1-FLAG-CtIP for 48 h, and MG132 (10 µM) was added 6 h before harvest. Cells were lysed using NP-40, and the insoluble fraction was removed by a high-speed spin. 1 mg of total cellular proteins of the clarified supernatant was subjected to immunoprecipitation using FLAG M2 beads (Sigma-Aldrich). CtIP ubiquitination was detected by immunoblotting analysis using an anti-ubiquitin antibody (Cell Signaling Technology).

Intracellular dNTP pool detection

The precold 80% (vol/vol) methanol was added to extract metabolites followed by centrifugation at 14,000 *g* for 10 min at 4°C. The dried supernatant was stored at −80°C until LC-MS/MS analysis. LC-MS/MS data were acquired using a TSQ Vantage triple-quadrupole mass spectrometer coupled to a Dionex Ultimate 3000 UHPLC system (Thermo Fisher Scientific). Chromatographic separation was performed on a SeQuant ZIC pHILIC column (2.1 × 150 mm, 5 µm; Merck) with a SeQuant ZIC pHILIC guard column (2.1 × 20 mm, 5 µm; Merck) at a flow rate of 250 µl/min. The mobile phase was composed of buffer A (20 mM ammonium hydroxide, 20 mM ammonium acetate in 95% [vol/vol] water, and 5% [vol/vol] acetonitrile, pH 9.0) and buffer B (100% acetonitrile). Gradient elution profile was 95% B (0.0–0.5 min) and 95% B to 40% B (0.5–21.0 min), and then reequilibration at 95% B for 9.0 min. The mass spectrometer was operated in negative selective reaction monitoring (SRM) mode. The ion spray voltage, vaporizer temperature, capillary temperature, sheath gas, and auxiliary gas pressure were set at 2,500 V, 300°C, 320°C, 40 arb, and 10 arb, respectively.

Intracellular NADPH/NADP$^+$ measurement

NADPH/NADP$^+$ kit (BioAssay Systems) was used to measure cellular NADPH/NADP$^+$ ratios. Cells were collected by a scraper, washed with PBS, and lysed with 200 µl of NADP$^+$ (or NADPH) extraction buffer. Heat extraction was allowed to proceed for 5 min at 60°C before adding 20 µl of assay buffer and 200 µl of the counter NADPH (or NADP$^+$) extraction buffer to neutralize the extracts. The supernatants were reacted with working buffer according to the manufacturer's protocol. The absorbance at 565 nm from the reaction mixture was measured with a plate reader.

Oxygen consumption rate and extracellular acidification rate analysis

Cells were planted into XF96 cell culture plates (Agilent Technologies). Each XF96 assay well was equipped with a disposable sensor cartridge and embedded with 96 pairs of fluorescent biosensors (oxygen and pH), coupled to fiber-optic waveguides. The measurement of oxygen consumption was expressed in picomoles per minute, and extracellular acidification rate was expressed in milli-pH per minute.

RNA isolation and RT-qPCR analysis

RNA from cell lines was isolated with TRizoland extracted using the RNeasy Mini kit according to the manufacturer's protocol (QIAGEN). Aliquots of 1 µg of total RNA were reverse-transcribed using ThermoScript RT-PCR System (Invitrogen). RT-qPCR was performed according to the instruction for SYBR Green PCR master mix (Applied Biosystems) with a V7 Real-Time PCR system (Applied Biosystems). Relative expression levels were calculated using the $2^{-\Delta\Delta CT}$ method. *β-actin* was used as the housekeeping gene for normalization. The sequences of primers used for qPCR analysis were as follows: CtIP (forward, 5′-AGATCGGTTAAGAGCAGGCTT-3′; reverse, 5′-GATTCT GCTGCCGGATATTT-3′); p21 (forward, 5′-AGCAGCGGAACAAGG AGT-3′; reverse, 5′-CGTTAGTGCCAGGAAAGACA-3′); and β-actin (forward, 5′-CATGTACGTTGCTATCCAGGC-3′; reverse, 5′-CTC CTTAATGTCACGCACGAT-3′).

ChIP assay

ChIP was performed using a SimpleChIP Plus Enzymatic Chromatin IP kit (#9005; Cell Signaling Technology) according to the

procedures provided by the manufacturer. The final ChIP DNAs were used as templates for qPCR reactions, using primers that encompass the *p21* promoter. The sequences of the primers were as follows: #1 (−1,339 to approximately −1,449), 5′-GGACTTGTCCCTAGGAAA AT-3′ and 5′-GAGTTTGCCCATGAGGGAGC-3′; #2 (−1,755 to approximately −1,863), 5′-GGAGCTAATAGATATCCACT-3′ and 5′-CTCTGCTAGGCATGAGTTGG-3′.

Animal studies

6- to 8-week-old nu/nu athymic BALB/c mice were obtained from Shanghai Laboratory Animal Center, Chinese Academy of Sciences (Shanghai, China). All studies were conducted in compliance with the Institutional Animal Care and Use Committee guidelines of Shanghai Institute of Materia Medica (Shanghai, China). Cells were suspended in PBS and injected into the right flank. Tumor-bearing mice were randomized into groups, and dosing began when mean tumor volume reached 100–200 mm^3. Olaparib (50 mg/kg) and PGMI-004A (50 mg/kg), alone or in combination, were injected daily for the indicated times. Tumor growth was monitored by the measurement of tumor size using calipers every 2 d by the formula (length × $width^2$)/2. Mice were killed, and tumor tissues were collected 2 h after the final dosing for immunoblotting or immunohistochemistry staining. Images of immunohistochemistry staining were captured using a BX51 microscope (Olympus) with a UPlanApo 20×/0.50 (Olympus) at RT and processed using DPController software.

Statistical analysis

Error bars represent mean ± SD of triplicates, or from six mice in each group for animal studies. Statistical significance was analyzed using two-tailed Student's *t* test or one-way analysis of variance, and $P < 0.05$ was considered statistically significant.

Online supplemental material

Fig. S1 shows the increased susceptibility to CPT and CDDP in PGAM1-depleted NCI-H1299 or CAL27 cells. Fig. S2 shows the subcellular localization of PGAM1 and compares cell viability of HeLa cells treated with CPT or CDDP alone or in combination with glycolytic inhibition. Fig. S3 shows PGAM1-modulated DSB end resection via affecting 6PGD and compares CtIP mRNA levels between cells transfected with indicated siRNAs. Fig. S4 shows the RPA foci and CtIP foci formation upon dNTP supplementation. Fig. S5 compares tumor weight, intratumoral 2-PG level, and body weight after Olaparib treatment, demonstrating that the combination of PGAM1 inhibitor sensitized BRCA proficient breast cancer toward PARP inhibitor.

Acknowledgments

We thank Drs. Maria Jasin and Hisao Masai for DR-U2OS cells and Drs. Dipanjan Chowdhury and Dong-Hyun Lee for NHEJ-HeLa cells.

This work was supported by the China International Science and Technology Cooperation Program (no. 2015DFM30040 to M. Huang), the National Science and Technology Major Project (no. 2015ZX09101009 to M. Huang), the Strategic Priority Research Program of the Chinese Academy of Sciences (no. XDA12020000 to M. Geng), the Natural Science Foundation of China for Innovation Research Group (no. 81321092 to J. Ding), and grants from the Natural Science Foundation of China (no. 81573464 to M. Huang and 21377106 to S. Lin).

The authors declare no competing financial interests.

Author contributions: M. Huang conceived the project and is responsible for all data, figures, and text; M. Geng and J. Ding provided supervision; J. Qu performed the research and analyzed the data; M. Zhu and M. Tan assisted with the proteomic study; J. Zhong and S. Lin assisted with the detection of dNTP levels; W. Sun, H. Lv, N. Jin, and Z. Xie conducted part of the experiments; J. Xu assisted with data analysis; and J. Qu and M. Huang wrote the manuscript. All authors approved the final version of the manuscript.

Submitted: 4 July 2016
Revised: 2 November 2016
Accepted: 17 January 2017

References

Aird, K.M., G. Zhang, H. Li, Z. Tu, B.G. Bitler, A. Garipov, H. Wu, Z. Wei, S.N. Wagner, M. Herlyn, and R. Zhang. 2013. Suppression of nucleotide metabolism underlies the establishment and maintenance of oncogene-induced senescence. *Cell Reports.* 3:1252–1265. http://dx.doi.org/10.1016/j.celrep.2013.03.004

Aparicio, T., R. Baer, M. Gottesman, and J. Gautier. 2016. MRN, CtIP, and BRCA1 mediate repair of topoisomerase II-DNA adducts. *J. Cell Biol.* 212:399–408. http://dx.doi.org/10.1083/jcb.201504005

Bensaad, K., A. Tsuruta, M.A. Selak, M.N. Vidal, K. Nakano, R. Bartrons, E. Gottlieb, and K.H. Vousden. 2006. TIGAR, a p53-inducible regulator of glycolysis and apoptosis. *Cell.* 126:107–120. http://dx.doi.org/10.1016/j.cell.2006.05.036

Brocklehurst, D., A.E. Champion, T.R. Cheek, and D.G. Dewhurst. 1986. The value of 6-phosphogluconate dehydrogenase (6-PGDH) activity as a marker of tumour cellularity and prognostic indicator in primary breast cancer. *Tumour Biol.* 7:99–104.

Chen, G., T.G. Gharib, H. Wang, C.C. Huang, R. Kuick, D.G. Thomas, K.A. Shedden, D.E. Misek, J.M. Taylor, T.J. Giordano, et al. 2003. Protein profiles associated with survival in lung adenocarcinoma. *Proc. Natl. Acad. Sci. USA.* 100:13537–13542. http://dx.doi.org/10.1073/pnas.2233850100

Cosentino, C., D. Grieco, and V. Costanzo. 2011. ATM activates the pentose phosphate pathway promoting anti-oxidant defence and DNA repair. *EMBO J.* 30:546–555. http://dx.doi.org/10.1038/emboj.2010.330

Dupuy, F., S. Tabariès, S. Andrzejewski, Z. Dong, J. Blagih, M.G. Annis, A. Omeroglu, D. Gao, S. Leung, E. Amir, et al. 2015. PDK1-dependent metabolic reprogramming dictates metastatic potential in breast cancer. *Cell Metab.* 22:577–589. http://dx.doi.org/10.1016/j.cmet.2015.08.007

Durany, N., J. Joseph, O.M. Jimenez, F. Climent, P.L. Fernández, F. Rivera, and J. Carreras. 2000. Phosphoglycerate mutase, 2,3-bisphosphoglycerate phosphatase, creatine kinase and enolase activity and isoenzymes in breast carcinoma. *Br. J. Cancer.* 82:20–27.

Egea, G., J.M. Ureña, X. Graña, J. Marsal, J. Carreras, and F. Climent. 1992. Nuclear location of phosphoglycerate mutase BB isozyme in rat tissues. *Histochemistry.* 97:269–275. http://dx.doi.org/10.1007/BF00267638

Fairbairn, D.W., P.L. Olive, and K.L. O'Neill. 1995. The comet assay: A comprehensive review. *Mutat. Res.* 339:37–59. http://dx.doi.org/10.1016/0165-1110(94)00013-3

Figueroa, M.E., O. Abdel-Wahab, C. Lu, P.S. Ward, J. Patel, A. Shih, Y. Li, N. Bhagwat, A. Vasanthakumar, H.F. Fernandez, et al. 2010. Leukemic IDH1 and IDH2 mutations result in a hypermethylation phenotype, disrupt TET2 function, and impair hematopoietic differentiation. *Cancer Cell.* 18:553–567. http://dx.doi.org/10.1016/j.ccr.2010.11.015

Flores, E.R., S. Sengupta, J.B. Miller, J.J. Newman, R. Bronson, D. Crowley, A. Yang, F. McKeon, and T. Jacks. 2005. Tumor predisposition in mice mutant for p63 and p73: Evidence for broader tumor suppressor functions for the p53 family. *Cancer Cell.* 7:363–373. http://dx.doi.org/10.1016/j.ccr.2005.02.019

Gut, P., and E. Verdin. 2013. The nexus of chromatin regulation and intermediary metabolism. *Nature.* 502:489–498. http://dx.doi.org/10.1038/nature12752

Hitosugi, T., L. Zhou, S. Elf, J. Fan, H.B. Kang, J.H. Seo, C. Shan, Q. Dai, L. Zhang, J. Xie, et al. 2012. Phosphoglycerate mutase 1 coordinates glycolysis and biosynthesis to promote tumor growth. *Cancer Cell.* 22:585–600. http://dx.doi.org/10.1016/j.ccr.2012.09.020

Hitosugi, T., L. Zhou, J. Fan, S. Elf, L. Zhang, J. Xie, Y. Wang, T.L. Gu, M. Alečković, G. LeRoy, et al. 2013. Tyr26 phosphorylation of PGAM1 provides a metabolic advantage to tumours by stabilizing the active conformation. *Nat. Commun.* 4:1790. http://dx.doi.org/10.1038/ncomms2759

Hsu, P.P., and D.M. Sabatini. 2008. Cancer cell metabolism: Warburg and beyond. *Cell.* 134:703–707. http://dx.doi.org/10.1016/j.cell.2008.08.021

Huang, M., J.M. Kim, B. Shiotani, K. Yang, L. Zou, and A.D. D'Andrea. 2010. The FANCM/FAAP24 complex is required for the DNA interstrand crosslink-induced checkpoint response. *Mol. Cell.* 39:259–268. http://dx.doi.org/10.1016/j.molcel.2010.07.005

Irwin, M.S., K. Kondo, M.C. Marin, L.S. Cheng, W.C. Hahn, and W.G. Kaelin Jr. 2003. Chemosensitivity linked to p73 function. *Cancer Cell.* 3:403–410. http://dx.doi.org/10.1016/S1535-6108(03)00078-3

Jeong, S.M., C. Xiao, L.W. Finley, T. Lahusen, A.L. Souza, K. Pierce, Y.H. Li, X. Wang, G. Laurent, N.J. German, et al. 2013. SIRT4 has tumor-suppressive activity and regulates the cellular metabolic response to DNA damage by inhibiting mitochondrial glutamine metabolism. *Cancer Cell.* 23:450–463. http://dx.doi.org/10.1016/j.ccr.2013.02.024

Jonas, S.K., C. Benedetto, A. Flatman, R.H. Hammond, L. Micheletti, C. Riley, P.A. Riley, D.J. Spargo, M. Zonca, and T.F. Slater. 1992. Increased activity of 6-phosphogluconate dehydrogenase and glucose-6-phosphate dehydrogenase in purified cell suspensions and single cells from the uterine cervix in cervical intraepithelial neoplasia. *Br. J. Cancer.* 66:185–191. http://dx.doi.org/10.1038/bjc.1992.240

Kumar, D., J. Viberg, A.K. Nilsson, and A. Chabes. 2010. Highly mutagenic and severely imbalanced dNTP pools can escape detection by the S-phase checkpoint. *Nucleic Acids Res.* 38:3975–3983. http://dx.doi.org/10.1093/nar/gkq128

Lafranchi, L., H.R. de Boer, E.G. de Vries, S.E. Ong, A.A. Sartori, and M.A. van Vugt. 2014. APC/C(Cdh1) controls CtIP stability during the cell cycle and in response to DNA damage. *EMBO J.* 33:2860–2879. http://dx.doi.org/10.15252/embj.201489017

Lin, Z.P., M.F. Belcourt, J.G. Cory, and A.C. Sartorelli. 2004. Stable suppression of the R2 subunit of ribonucleotide reductase by R2-targeted short interference RNA sensitizes p53(-/-) HCT-116 colon cancer cells to DNA-damaging agents and ribonucleotide reductase inhibitors. *J. Biol. Chem.* 279:27030–27038. http://dx.doi.org/10.1074/jbc.M402056200

Maréchal, A., and L. Zou. 2015. RPA-coated single-stranded DNA as a platform for post-translational modifications in the DNA damage response. *Cell Res.* 25:9–23. http://dx.doi.org/10.1038/cr.2014.147

Matsuoka, S., B.A. Ballif, A. Smogorzewska, E.R. McDonald III, K.E. Hurov, J. Luo, C.E. Bakalarski, Z. Zhao, N. Solimini, Y. Lerenthal, et al. 2007. ATM and ATR substrate analysis reveals extensive protein networks responsive to DNA damage. *Science.* 316:1160–1166. http://dx.doi.org/10.1126/science.1140321

Nakamura, K., T. Kogame, H. Oshiumi, A. Shinohara, Y. Sumitomo, K. Agama, Y. Pommier, K.M. Tsutsui, K. Tsutsui, E. Hartsuiker, et al. 2010. Collaborative action of Brca1 and CtIP in elimination of covalent modifications from double-strand breaks to facilitate subsequent break repair. *PLoS Genet.* 6:e1000828. http://dx.doi.org/10.1371/journal.pgen.1000828

Ogiwara, H., A. Ui, A. Otsuka, H. Satoh, I. Yokomi, S. Nakajima, A. Yasui, J. Yokota, and T. Kohno. 2011. Histone acetylation by CBP and p300 at double-strand break sites facilitates SWI/SNF chromatin remodeling and the recruitment of non-homologous end joining factors. *Oncogene.* 30:2135–2146. http://dx.doi.org/10.1038/onc.2010.592

Pierce, A.J., R.D. Johnson, L.H. Thompson, and M. Jasin. 1999. XRCC3 promotes homology-directed repair of DNA damage in mammalian cells. *Genes Dev.* 13:2633–2638. http://dx.doi.org/10.1101/gad.13.20.2633

Quennet, V., A. Beucher, O. Barton, S. Takeda, and M. Löbrich. 2011. CtIP and MRN promote non-homologous end-joining of etoposide-induced DNA double-strand breaks in G1. *Nucleic Acids Res.* 39:2144–2152. http://dx.doi.org/10.1093/nar/gkq1175

Sanzey, M., S.A. Abdul Rahim, A. Oudin, A. Dirkse, T. Kaoma, L. Vallar, C. Herold-Mende, R. Bjerkvig, A. Golebiewska, and S.P. Niclou. 2015. Comprehensive analysis of glycolytic enzymes as therapeutic targets in the treatment of glioblastoma. *PLoS One.* 10:e0123544. http://dx.doi.org/10.1371/journal.pone.0123544

Sartori, A.A., C. Lukas, J. Coates, M. Mistrik, S. Fu, J. Bartek, R. Baer, J. Lukas, and S.P. Jackson. 2007. Human CtIP promotes DNA end resection. *Nature.* 450:509–514. http://dx.doi.org/10.1038/nature06337

Shao, R.G., C.X. Cao, H. Zhang, K.W. Kohn, M.S. Wold, and Y. Pommier. 1999. Replication-mediated DNA damage by camptothecin induces phosphorylation of RPA by DNA-dependent protein kinase and dissociates RPA:DNA-PK complexes. *EMBO J.* 18:1397–1406. http://dx.doi.org/10.1093/emboj/18.5.1397

Symington, L.S. 2002. Role of RAD52 epistasis group genes in homologous recombination and double-strand break repair. *Microbiol. Mol. Biol. Rev.* 66:630–670. http://dx.doi.org/10.1128/MMBR.66.4.630-670.2002

Thelander, M., A. Gräslund, and L. Thelander. 1985. Subunit M2 of mammalian ribonucleotide reductase. Characterization of a homogeneous protein isolated from M2-overproducing mouse cells. *J. Biol. Chem.* 260:2737–2741.

Turcan, S., D. Rohle, A. Goenka, L.A. Walsh, F. Fang, E. Yilmaz, C. Campos, A.W. Fabius, C. Lu, P.S. Ward, et al. 2012. IDH1 mutation is sufficient to establish the glioma hypermethylator phenotype. *Nature.* 483:479–483. http://dx.doi.org/10.1038/nature10866

Tutt, A., M. Robson, J.E. Garber, S.M. Domchek, M.W. Audeh, J.N. Weitzel, M. Friedlander, B. Arun, N. Loman, R.K. Schmutzler, et al. 2010. Oral poly(ADP-ribose) polymerase inhibitor olaparib in patients with BRCA1 or BRCA2 mutations and advanced breast cancer: A proof-of-concept trial. *Lancet.* 376:235–244. http://dx.doi.org/10.1016/S0140-6736(10)60892-6

Vander Heiden, M.G. 2011. Targeting cancer metabolism: A therapeutic window opens. *Nat. Rev. Drug Discov.* 10:671–684. http://dx.doi.org/10.1038/nrd3504

Vayssade, M., H. Haddada, L. Faridoni-Laurens, S. Tourpin, A. Valent, J. Bénard, and J.C. Ahomadegbe. 2005. P73 functionally replaces p53 in Adriamycin-treated, p53-deficient breast cancer cells. *Int. J. Cancer.* 116:860–869. http://dx.doi.org/10.1002/ijc.21033

Wang, J., Q. Ding, H. Fujimori, A. Motegi, Y. Miki, and M. Masutani. 2016. Loss of CtIP disturbs homologous recombination repair and sensitizes breast cancer cells to PARP inhibitors. *Oncotarget.* 7:7701–7714. http://dx.doi.org/10.18632/oncotarget.6715

Ward, P.S., and C.B. Thompson. 2012. Metabolic reprogramming: A cancer hallmark even Warburg did not anticipate. *Cancer Cell.* 21:297–308. http://dx.doi.org/10.1016/j.ccr.2012.02.014

Wellen, K.E., G. Hatzivassiliou, U.M. Sachdeva, T.V. Bui, J.R. Cross, and C.B. Thompson. 2009. ATP-citrate lyase links cellular metabolism to histone acetylation. *Science.* 324:1076–1080. http://dx.doi.org/10.1126/science.1164097

Wiebusch, L., and C. Hagemeier. 2010. p53- and p21-dependent premature APC/C-Cdh1 activation in G2 is part of the long-term response to genotoxic stress. *Oncogene.* 29:3477–3489. http://dx.doi.org/10.1038/onc.2010.99

Williams, L.N., L. Marjavaara, G.M. Knowels, E.M. Schultz, E.J. Fox, A. Chabes, and A.J. Herr. 2015. dNTP pool levels modulate mutator phenotypes of error-prone DNA polymerase ε variants. *Proc. Natl. Acad. Sci. USA.* 112:E2457–E2466. http://dx.doi.org/10.1073/pnas.1422948112

Willis, A.C., T. Pipes, J. Zhu, and X. Chen. 2003. p73 can suppress the proliferation of cells that express mutant p53. *Oncogene.* 22:5481–5495. http://dx.doi.org/10.1038/sj.onc.1206505

Wu, C.C., T.K. Li, L. Farh, L.Y. Lin, T.S. Lin, Y.J. Yu, T.J. Yen, C.W. Chiang, and N.L. Chan. 2011. Structural basis of type II topoisomerase inhibition by the anticancer drug etoposide. *Science.* 333:459–462. http://dx.doi.org/10.1126/science.1204117

Yogev, O., O. Yogev, E. Singer, E. Shaulian, M. Goldberg, T.D. Fox, and O. Pines. 2010. Fumarase: A mitochondrial metabolic enzyme and a cytosolic/nuclear component of the DNA damage response. *PLoS Biol.* 8:e1000328. http://dx.doi.org/10.1371/journal.pbio.1000328

Yu, H.P., J.M. Xie, B. Li, Y.H. Sun, Q.G. Gao, Z.H. Ding, H.R. Wu, and Z.H. Qin. 2015. TIGAR regulates DNA damage and repair through pentosephosphate pathway and Cdk5-ATM pathway. *Sci. Rep.* 5:9853. http://dx.doi.org/10.1038/srep09853

Zhang, D., N. Jin, W. Sun, X. Li, B. Liu, Z. Xie, J. Qu, J. Xu, X. Yang, Y. Su, et al. 2016. Phosphoglycerate mutase 1 promotes cancer cell migration independent of its metabolic activity. *Oncogene*. http://dx.doi.org/10.1038/onc.2016.446

Zhao, R., K. Gish, M. Murphy, Y. Yin, D. Notterman, W.H. Hoffman, E. Tom, D.H. Mack, and A.J. Levine. 2000. Analysis of p53-regulated gene expression patterns using oligonucleotide arrays. *Genes Dev.* 14:981–993.

Zhao, Y., E.B. Butler, and M. Tan. 2013. Targeting cellular metabolism to improve cancer therapeutics. *Cell Death Dis.* 4:e532. http://dx.doi.org/10.1038/cddis.2013.60